The State-of-the-Practice of Modern Structural Health Monitoring for Bridges: A Comprehensive Review

T. M. Ahlborn, Ph.D., P.E.[1], R. Shuchman Ph.D[2], L. L. Sutter Ph.D.[1], C. N. Brooks[2], D. K. Harris, Ph.D.[1], J. W. Burns Ph.D[2], K. A. Endsley[2], D. C. Evans[1], K. Vaghefi[1], R. C. Oats[1]

[1]Department of Civil and Environmental Engineering
Michigan Tech Transportation Institute
Michigan Technological University
1400 Townsend Drive
Houghton, Michigan USA 49931
(906) 487-2625; fax (906) 487-1620; email: tess@mtu.edu

[2]Michigan Tech Research Institute
Michigan Technological University
3600 Green Court, Suite 100
Ann Arbor, Michigan USA 48105
(734) 913-6840; fax (734) 913-6880; email: cnbrooks@mtu.edu

June 30, 2010

Michigan Tech

Table of Contents

Abstract

Since the National Bridge Inventory (NBI) was first conducted, structural health monitoring (SHM) of the United States bridge infrastructure has consisted largely of labor-intensive, subjective measures like chain dragging and the tap test. Recent developments in a variety of sensor technologies and an improvement of computing and networking capabilities have allowed for the installation of in-situ sensor networks responsible for monitoring—among other parameters—the strain and deformation of structural members and concrete deck cracking. These relatively new techniques are quite costly, however, and in many cases are infeasible for SHM because they require installation in hard-to-reach places or during construction, limiting their application to the small number of bridges being built today compared to the current population of in-service bridges. Stand-off SHM techniques such as radar, electro-optical, laser scanning and other remote sensing technologies may offer an innovative, cost-effective method of monitoring the dynamic conditions of U.S. bridges in real-time. This paper investigates the state of the practice of SHM and provides summaries of existing technologies, both in-situ sensors and networks and remote techniques, as well as case studies of instrumented bridges.

Acknowledgements

This work is supported by the Commercial Remote Sensing and Spatial Information program of the Research and Innovative Technology Administration (RITA), U.S. Department of Transportation (USDOT), Cooperative Agreement # DTOS59-10-H-00001, with additional support provided by the Michigan Department of Transportation, the Michigan Tech Transportation Institute, the Michigan Tech Research Institute, and the Center for Automotive Research. The views, opinions, findings, and conclusions reflected in this paper are the responsibility of the authors only and do not represent the official policy or position of the USDOT, RITA, or any state or other entity. Additional information regarding this project can be found at www.mtti.mtu.edu/bridgecondition .

5.0 Overview

The transportation infrastructure of the United States is in need of rehabilitation and repair. According the American Society of Civil Engineers (ASCE), more than 27% of the nation's bridges are either structural deficient or functionally obsolete. One succinct and startling statistic is that the average American bridge is now 43 years old. The ASCE estimates that the total investment needed to bring the nation's bridge infrastructure up to code over 5 years is 930 billion dollars, but in that time only $549.5 billion is projected to be spent (ASCE 2009). With a finite amount of funding, the allocation of such funds may make up the difference in the long run. Rehabilitation, for instance, is far cheaper than replacement when damage is minor. Better management of funds used to inspect and maintain existing bridge infrastructure could reduce costs. A report by the Federal Highway Administration indicates that, given more time and funding to complete bridge inspections, the use of non-destructive evaluation (NDE) methods would increase by state and county transportation agencies (USDOT 2001). NDE promises a way to improve the allocation of funding by improving the information these decisions are based on, by improving the assessment of existing bridge conditions.

Currently, structural health monitoring (SHM) in the United States and most other developed nations is characterized by traditional visual inspection along with referencing of old inspection reports to maintain an accurate account of the bridges condition. The standard evaluations used by the Federal Highway Administration have been limited to auditory tests and visual inspection since the National Bridge Inventory (NBI) was first conducted (Chong et al. 2003) almost 40 years ago. The NBI has its roots in the Federal Highway Act of 1968, which was enacted following the tragic collapse of the Silver Bridge in Ohio. Krajewski (2006), an excellent reference that reads like a history of bridge inspection, describes the training and resources provided to bridge inspectors as part of the federal initiative. The program emphasizes visual inspection techniques with manuals that provide photographs of the various types and degrees of deterioration in bridge elements. Bridge inspectors are trained in identifying all the types of deterioration, but there is a subjective component when dealing with the rating of the bridges. The NBI uses a rating system of zero to nine for the rating of the condition of the bridge to system to allow for uniform characterization of bridge condition.

Traditional slow and subjective methods used in assessing deck condition, which include impact sounding, chain dragging, half-cell potential, and core analysis, are being replaced by more modern techniques. The use of remote sensing techniques and robust, permanent sensor networks on bridges are being investigated. As of 2005, about 40 long-span (100 m or longer) bridges worldwide have been equipped with sophisticated health monitoring instrumentation systems. These systems are lauded as "array[s] of inexpensive, spatially distributed, wirelessly powered, wirelessly networked, embedded sensing devices supporting frequent and on-demand acquisition of real-time information about the loading and environmental effects, structural characteristics, and responses" (Ko and Ni 2005). Despite these advantages, permanent, in-situ sensor networks are costly and can be difficult to install on some bridges or bridge elements, particularly when they were not considered during the construction phase.

Permanent networks of sensors are deployed on bridges with two distinct goals in mind: the generation of alerts for bridge managers and the viewing/analysis of continuous real-time structural data. These goals are achieved by networks that emphasize two discriminating factors: the time-scale of the change and the severity of the change. Traditionally, these networks have consisted of in-situ sensors coupled with structural elements and wired to both a data-acquisition system and a power source. Consequently, these networks are costly, cumbersome, and in some cases interrupt the normal operation of the structure (Kim et al. 2007).

In-situ sensor networks paved the way for modern bridge monitoring practices, including electronic data collection and distribution. Bridge inspection officials have indicated that the best way to improve the performance of bridge inspections is to allow for electronic data to be uploaded directly to a Bridge Management System; many have also cited the establishment of such a system as a major accomplishment for their team (USDOT 2001). This is a popular idea in most conceptions of modern bridge monitoring by large, disseminated networks of permanent, in-situ sensors. Ideally, SHM should incorporate remote sensing techniques that provide the same capability for the remote collection of high-resolution (both spatial and temporal), real-time structural data without the need for costly hardware and its installation, calibration, and maintenance. In this paper, modern in-situ techniques (where sensors are in direct-contact with bridge elements), on-site surveys (where instrumentation is brought to the bridge to make measurements), as well as standoff remote sensing techniques (where remote sensors are used far from the bridge) for the SHM of bridges are summarized.

In its 1998 survey, the Federal Highway Administration (FHWA) surveyed the use of NDE techniques for SHM among state and Iowa county DOTs as well as independent contractors. From the 14 (out of 42) state DOT respondents, they learned that the most common NDE techniques being employed in the field (by ASNT Level III personnel) were liquid penetrant testing, ultrasonic testing, and magnetic particle testing with a smaller number reporting expertise in radiographic and electromagnetic techniques. All of these techniques increased in reported use from 1993 to 1998 according to three different surveys. Citing a similar survey from 1994, the FHWA concluded, from an increase of 19 to 33 percent response, that use of the American Society for Non-destructive Testing (ASNT) Level III certification has increased (USDOT 2001). Visual inspection dominated among NDE techniques then being used on existing bridges of all types, followed by the aforementioned techniques for steel bridges. On concrete bridges, mechanical sounding was second to visual inspection, followed by some innovation such as electrical potential and radar measurements. While many state DOTs reported a variety of advanced NDE techniques such as these being used, almost no county or local agencies reported using anything other than visual techniques and mechanical sounding. Of the state transportation agencies that use advanced NDE techniques, some indicated that they had ceased using techniques such as ultrasonic testing of pin/hanger connections, various pile testing, radar, and acoustic emissions due to unreliable performance or other reasons.

It is important to describe modern instrumentation in detail. For both remote and in-situ instrumentation, traditional and modern techniques can be broken down into two distinct categories of monitoring. While "local" health monitoring methods are used to precisely determine the location and extent of damage, "global" methods can only determine damage of the structure as a whole (Chang et al. 2003). Both are equally valuable, as global methods easily and quickly establish that damage has occurred to the structure. Local methods would not be used to initially assess whether damage has occurred, but are necessary for isolating exactly where known damage exists. In all SHM practice, the first step should be to determine what parameters need to be measured, as this will determine what methods are used. For concrete bridges the most critical parameters are strain, temperature, cracking of concrete, and corrosion of reinforcement (Casas and Cruz 2003).

Modern global health monitoring techniques rely on finding shifts in resonant frequencies or changes in structural mode shapes. The challenge with these modern techniques is to differentiate real structural damage from environmental factors such as moisture and temperature by distinguishing significant shifts from the background (Chang et al. 2003). Stress-wave propagation, for example, is a promising global, non-destructive evaluation (NDE) for concrete structures and has been employed with great success where it involves mechanical impacts (Chong et al. 2003). Ground-penetrating radar (GPR) and infrared thermography have also been cited as the most promising emerging techniques for bridge monitoring (Maser and Roddis 1990), especially in the evaluation of a bridge's concrete deck (traffic surface). Reinforced concrete decks have a far shorter life span than the finite elements or bridge superstructure, and as such deserve special attention.

Chang et al. (2003) also describes several innovative monitoring techniques for local SHM including micro-electromechanical system (MEMS) devices for accelerometers and velocimeters, nuclear magnetic resonance (NMR) for the detection of chloride intrusion, as well as shearography and LiDAR. Two major areas of interest with respect to the SHM of bridges are crack detection and inspection of the concrete deck (traffic surface). Visual techniques and dye penetration have historically been used for crack detection but new electromagnetic methods including the use of eddy currents and radar (ground-penetrating, interferometric, microwave) as well as acoustic methods (ultrasonic, acoustic impedance, and acoustic attenuation) can also be employed. Electro-optical imaging techniques are also promising as cracks reflect and absorb light differently than intact regions. Piezoelectric wafers are deployed at problem areas and relied upon to produce signals which indicate when cracks and degradation take place. Other innovative techniques for SHM include X-ray and Gamma-ray imaging for steel cables and slabs. Fiber optic sensors allow for complex, distributed networks of sensors capable of detecting cracks in concrete, the presence of chloride ions, or corrosion of reinforcing steel. Chang et al. (2003) distinguishes these multifarious NDE techniques categorically: acoustic signals, electromagnetic, radiography (X-ray and Gamma ray), fiber optics, radar and radio frequency, optics (TLS and LiDAR), and piezoelectric detectors of acoustic impedance. This is how these techniques are classified in this paper, though some are given more emphasis than others based on their perceived acceptance and use in industry.

A report (USDOT 2001) by the Federal Highway Administration's Turner-Fairbank Highway Research Center details the state of routine bridge inspection practice as of 2001. Using the results of a survey they conducted and the results of 42 state Departments of Transportation (DOTs), 72 Iowa county DOTs, and 15 bridge inspection contractors, they profiled the activities of these agencies in the U.S. They found that more than 90% of state DOTs conducted bridge surveys with their own employees as well as contractors while half of Iowa county DOTs relied solely on contractors. The services that contractors performed included the inspection of moveable bridges, ultrasonic testing of hanger pins, scour analysis, fracture-critical inspections, and complex traffic control; two state DOT respondents also indicated they hired contractors when the agency was behind schedule. The authors provided an example of a specific bridge type (20-years old, two-span, two-lane, steel, four-girder bridge with welded flange cover plates, concrete deck and abutments, and a single three-column concrete pier with pier cap) and found that the average time for state and county DOTs to perform such a bridge inspection is 4.5 man-hours; about 2 people are usually assigned. The authors also found that while 83% of contractors who responded have a Professional Engineer (PE) on-site for 81-100% of their bridge inspections, about half of state and county DOTs rarely, if ever, have a PE on-site. When a PE is present, it is usually either because they are a routine member of the inspection team or because a follow-up inspection is being performed. Fracture-critical and closure conditions are also cases in which a PE is likely to be deployed for bridge inspection. State and county agencies listed the areas in which they would allocate additional time and money for bridge inspections were it available. The most common responses included the increased use of NDE, additional personnel and equipment, improvements to their Bridge Management System, and an increase in the amount of time allowed for inspection.

All of the respondents—county and state DOTs and contractors—indicated that previous inspection reports for a bridge were made available both before the inspector arrived and also at the bridge site. Results from the survey indicate that state DOTs inspect, on average, 6,300 bridges per year while county DOTs and contractors inspect 240 and 820 bridges per year, on average, respectively. However, bridge inspection counts from the Iowa county DOTs seem too high in light of the total number of bridges in Iowa. The most common quality assurance/quality control (QA/QC) measures taken include an office review of inspection reports, rotation of bridge inspectors, field re-inspection programs, and "ride-alongs" by a PE on bridge inspections in conjunction with a field review.

2.0 Bridge Evaluation Process

2.1 Inspection Basics

The performance evaluation of bridges starts with the inspection of the bridge to determine the present condition. This is completed in a variety of ways depending on the particular personnel and department conducting the inspection of the bridge, but all inspections are completed in accordance with the National Bridge Inspection Standards (NBIS). The Bridge Inspector's Reference Manual (BIRM) aids the bridge inspector with programs, procedures, and techniques for inspecting and evaluating a variety of in-service highway bridges (Ryan et al 2006). The BIRM is sponsored by the National Highway Institute for the Federal Highway Administration (FHWA). Before an inspector is qualified for the inspecting of bridges they are required to attend an inspection course that satisfies the requirement of the NBIS for a comprehensive training program. This is typically a one to two week course depending on the background of the inspector and types of inspections to be completed. To determine the overall condition of a bridge inspectors follow the guidelines provided for them, but also include personnel or experience based judgment when assigning a rating for a particular bridge. This is where concern can come into play with structural health monitoring because of the limited consistency from one inspector's rating to the next inspector's rating.

According to NBIS, bridges must be inspected at least every two years. Some bridges with problem areas at the discretion of the owner may need to be inspected more frequently than two year minimum required. Any structure that has a span length of greater than twenty feet as defined by the NBIS regulations is required to be rated for National Bridge Inventory (NBI). There are currently 603,248 bridges rated within the NBI system as of December 2009. The number of bridges listed as structurally deficient as of 2009 was 71,179 (11.8%) and 78,462 (13.0%) were classified as functionally obsolete, demonstrating the need for a uniform rating system to ensure the correct bridges receive the appropriate attention and funding (Federal Highway Administration).

A general rating system is used to classify the condition on a 9 to 0 scale with 9 being a new bridge and 0 being out of service. A structurally deficient bridge would be rated at a “4” (poor) or less for superstructure, deck and/or substructure. A structurally deficient bridge could also have waterway adequacy that is rated at a “2” or less. Structural deficient bridges cannot support the intended traffic loads which results in postings to reduce weight and/or speed on the structure. In contrast functionally obsolete bridges do not typically represent a safety threat, but typically no longer have an adequate approach alignment, geometry or clearance for the given traffic needs and are below current design standards (Amey 2009).

2.2 Visual Inspection

BIRM states the typical routine inspection performed for the bridge would be a review of the previous inspection and a visual inspection of all the different members from on top of the bridge and underneath the bridge. The second type of visual inspection would be the in-depth inspection of one or more elements at less than an arm's length from the inspector. With a visual inspection of the bridge, the inspector would be looking for various distress or signs of those defects in the different members of the structure. If a defect is seen or suspected the inspector will often perform other inspection techniques to determine the extent of the defect on the structure. The location of fracture critical members is important when performing an inspection because these are often non-redundant members in the structure. The inspector pays particularly close attention to ensure that any defect that could potentially affect the capacity of a member or the bridge overall is closely inspected.

2.3 Defects

Bridges are designed with a variety of materials with the three main materials being concrete, steel and timber. Each of these materials has special characteristic that determine which types of defects that the inspector must monitor to confirm the material still has adequate remaining useful life for the member being inspected. The NBI is composed of 64.3% of concrete bridges and 30.9% of steel bridges. The use of timber is limited with about 4.2% of bridges being classified as a timber bridges along with only 0.3% of bridges being masonry (Federal Highway Administration). Table 1 shows the defects according to BIRM for the different materials that compose the different structural elements of the bridge. These defects are often associated with one or more structural groupings including deck, superstructure or substructure.

Table 1: Material Defects

Material	Defects
Concrete	cracking, scaling, delamination, spalling, chloride contamination, efflorescence, ettringite formation, honeycombs, pop-outs, wear, collision damage, abrasion, overload damage, reinforcing steel corrosion, prestressed concrete deterioration.
Steel	corrosion, fatigue cracking, overloads, collision damage, heat damage, paint failures
Timber	natural defects, decay, insects, chemical contamination, delaminations, loose connections, fire damage, weathering, warping, protective coating failure
Masonry	weathering, spalling, splitting, fire damage

When inspecting the deck of the bridge the inspector will look for key defects over the entire bridge. Of primary importance are the defects that affect ride quality of the bridge deck because the public often only feels irregularities from the riding surface. BIRM states that the inspector is typically looking for unevenness, settlement and roughness when determining the condition of the deck. Spalling is one of the defects that inspectors take into account with the safety of cars being of concern with falling concrete. Cracking is also of concern with rebar being exposed to elements possibly causing corrosion. Also the condition of the expansion joint is considered with the inspection of the deck. If there is a problem with the expansion joint could lead to superstructure degradation or alert the inspector to possible other damage in the bridge deck. The evaluation of bridge deck deterioration prompts deck repair, rehabilitation and replacement decisions. Sometimes asphalt is used to overlay the deck the bridge inspector would then have to look for other signs of distress in the deck below the overlay.

The superstructure is of particular importance from a safety perspective, to ensure that the members are adequate for the loads supported by these members. The inspection of the superstructure is searching for any of the defects in structural members. Some of the main defects that an inspector is looking for are exposed reinforcement, steel section loss and frozen bearing. The inspector should also confirm that the given members match those from plans. Additionally the bearing supports should also be checked thoroughly to ensure critical members are appropriately transferring the load from the superstructure to the substructure.

The substructure also has to be inspected for several different issues to be assured that it is not approaching failure. Some of the main defects the inspector would be looking for in the substructure members would be degradation, exposed rebar, cracking and corrosion. BIRM states that the inspector should determine the dimensions of the substructure to compare to those of the plan. Additionally, settlement of the substructure should be checked. According to BIRM this can be completed by looking along the superstructure to see if any of the vertical faces are tilting. Inspection of the substructure is typically finished with checking for scour or undermining of the structure.

2.4 Traditional Inspection Tools

BIRM suggests several tools that the inspector could use while performing the inspection to insure an accurate assessment of the structure's condition. The inspector should carry tools to clear debris (broom, wire brush, scraper, flat bladed screwdriver and shovel), and an inspection hammer for sounding concrete, checking for sheared or loose connections and loosening dirt and debris. The inspection hammer can be used by the trained inspector to determine the condition of member by the sound produced by tapping the hammer to the material. A chain drag apparatus is often used to determine the location of any delaminations that are located in the concrete bridge deck. The chains produce a clear ringing sound in areas where there are no delaminations and produce a dull or hollow sound where there is a delamination in the concrete (Scheff and Chen 2000); however this technique is ineffective where asphalt overlays are applied.

2.5 Advanced Inspection Techniques

When evaluation beyond the aforementioned basic techniques is required, more advanced inspections are typically performed. These advanced techniques often require specialized equipment and may require specialized personnel. The different types of inspection techniques available are numerous and are constantly evolving, but can generally be categorized into two types, destructive and nondestructive. A summary of these different techniques listed in BIRM can be seen in Table 2. The purpose of a nondestructive test is to determine characteristics such as: strength and location of abnormalities, without compromising the integrity of the structure. This is important when inspecting a bridge because the less destructive tests required the better the structure will maintain its integrity. Destructive tests can affect the integrity of the structure, so the amount of testing is typically limited. Also the time required for destructive tests is extensive, often requiring the material samples to be delivered to a lab for testing. As a result, destructive tests are often used to confirm the findings of a nondestructive test. A typical example of confirmation destructive testing would be coring of concrete to confirm location and degree of delamination observed from an IR survey. Each individual test provides different information, so the inspector should use discretion for what test to use for the given situation.

Table 2: Bridge Testing Methods

Material	Test Type	Tests
Steel	Nondestructive	acoustic emissions testing, corrosion sensors, smart paint, dye penetrant, magnetic particle, radiographic testing, computer tomography, ultrasonic testing, eddy current
Steel	Destructive	Brinell hardness test, Charpy impact test, tensile strength test
Concrete	Nondestructive	acoustic wave sonic, delamination detection machinery, ground-penetrating radar, electromagnetic methods, pulse velocity, flat jack testing, impact-echo testing, infrared thermography, laser ultrasonic testing, magnetic field disturbance, nuclear methods, pachometer, rebound and penetration methods ultrasonic testing
Concrete	Destructive	core sampling, carbonation, concrete permeability, concrete strength, endoscopes, videoscopes, moisture content, reinforcing steel strength, petrographic examination
Timber	Nondestructive	Pol-Tek, spectral analysis, ultrasonic testing, vibration
Timber	Destructive	boring, drilling, moisture content, probing, shigometer

2.6 Condition Rating

The rating of the condition of the three main components is done on a scale of zero to nine according to the Recording and Coding Guide for the Structure Inventory and Appraisal of the Nation’s Bridges (Federal Highway Administration 1995). This guide was created to help promote uniformity in bridge structure rating. The bridge section of this guide is located between Items 58 to 62. A detailed guide of what each rating of a structure stands for with a nine standing for excellent condition and a zero being failed condition out of service. The rating of the deck members that are integral with the superstructure are to be rated as a deck only not on how it influences the superstructure. Rating the deck, superstructure and substructure separately allows for an overall view of where the structural deficiencies are occurring. These ratings are then placed into the Pontis database system which forms the annual basis of the National Bridge Inventory (NBI). This inventory/rating database allows the federal government to get an accurate account of the condition of the United States bridge system. The rating system is key to providing a high-level summary of how and where work is need on the system of bridges and prioritizing funding on a national level.

Table 3: Condition Ratings

Rating	Definition	Description
9	Excellent Condition	
8	Very Good Condition	No problems noted
7	Good Condition	Some minor problems
6	Satisfactory Condition	Structural elements show some minor deterioration
5	Fair Condition	All primary structural elements are sound but may have some minor section loss, cracking, spalling or scour
4	Poor Condition	Advanced section loss, deterioration, spalling or scour
3	Serious Condition	Loss of section, deterioration, spalling or scour have seriously affected primary structural components. Local failures are possible. Fatigue cracks in steel or shear cracks in concrete may be present.
2	Critical Condition	Advanced deterioration of primary structural elements. Fatigue cracks in steel or shear cracks in concrete may be present or scour may have removed substructure support. Unless closely monitored it may be necessary to close the bridge unless corrective action is taken.
1	“Imminent” Failure Condition	Major deterioration or section loss present in critical structural components or obvious vertical or horizontal movement affecting structural stability. Bridge closed to traffic but corrective action may put it in light service.
0	Failed Condition	Out of service – beyond corrective action

3.7 Load Rating Another important rating criteria is load rating which defines the load limit on the structure to prevent catastrophic failure. There are two different rating levels that the New Mexico Department of Transportation uses when applying load ratings to a bridge inventory and operating levels. The inventory level represents the live load that a bridge can safely sustain for an indefinite period of time, whereas the operating level defines the level of permit load allowed across the bridge (Castro et al. 2009). According to The Manuel for Bridge Evaluation (MBE, 2008) there are three distinct procedures for the load and resistance factor rating of bridges: design load rating, legal road rating and permit load rating. The design load is a measure of how the bridge in its current condition performs under current LRFD bridge design standards. If the bridge can support all the LRFD limit states the bridge would be satisfactory for legal loads. The legal load rating considers the effect of legal loaded truck traffic on the bridge. This can be the basis for posting load limits on the bridge or a bridge strengthening project. Permit load rating would be to check the effects of an overweight vehicle would have on the bridge taking into consideration the different factors on an individual permit basis.

3.0 In-Situ Monitoring Techniques

3.1 Accelerometers and Velocimeters

Accelerometers are relatively simple devices that compare the acceleration they experience to the acceleration due to gravity and are commonly provided as microelectro-mechanical systems (MEMS)—tiny machines with computing power. Velocimeters typically work through the same principles as interferometry. In SHM, both are primarily used for measuring displacement—through the integration of acceleration or velocity measurements—of structural members they are attached to. As the second derivative of displacement, however, acceleration can never provide information about the absolute position of the structure making it useless for detecting differential settlements, leaning, or any permanent offsets (Kijewski-Correa 2005). GPS may provide absolute positioning, but even when it is used to inform accelerometer measurements, the second integral of acceleration provides larger relative displacements than those provided by GPS due to scale factor errors and sensor biases. In addition, the signal noise of an accelerometer is device-specific and all have a band-pass frequency response including significantly poor performance at vibration frequencies lower than 0.2 Hz which prohibits their application to long-span bridges (Meng et al. 2007).

Accelerometers have been used for their ability to detect higher-frequency vibrations, particularly those that cannot be monitored by GPS. These vibrations are either the result of ambient or forced bridge loading. Ambient movements are those which abound during the everyday life of the bridge; the results of traffic, wind, and water. Forced movements are specific loads applied to the bridge as tests for the purpose of measuring its response. Due to the cost of forced movement on long-span bridges and because it is virtually identical to the ambient movement of long-span bridges, it is generally not practiced (Meng et al. 2007).

Accelerometers have been used to monitor rigidly bolted joints for damage (Tanner et al. 2003) and could be used more generally to monitor the 3D displacement of large structural elements due to wind or load variance in real time. Accelerometers are also used in conjunction with innovative signal processing and time-series analysis for global SHM—the assessment of whether or not a structure has been damaged (Lynch et al. 2006). They are currently the convention for dynamic testing or monitoring of large structures and have also been recognized for their efficacy in studies comparing new SHM methods against them (Hide et al.; Lynch et al. 2006; Gueguen et al. 2009). The ubiquity of accelerometers in SHM is shown by their use in studies examining more general aspects of SHM, in particular the shift from wired to wireless sensor arrays, such as in Whelan et al. (2007), Lynch and Loh (2006), and Masri et al. (2004). They can obtain accuracies in acceleration measurements on the order of milligrams of loading (Lee et al. 2005).

3.2 Electrical Resistance

The electrical resistance method of SHM is a global, on-site, de-coupled technique for detecting defects even of modest size in composite materials and joints. Carbon-fiber polymer-matrix composites have been demonstrated to be a viable material for monitoring with this method, as they exhibit electrical properties which are affected by structural damage (Chung 2001). In addition, they are extremely strong, super-elastic, and possess piezoresistive qualities (Kang et al. 2006). In particular, as the conductivity in a certain direction of these composites is dependent on the number of carbon-fiber contacts, cracking can be detected by examination of the conductance (inverse of resistance) and its material characteristic, conductivity (inverse of resistivity). In general, fiber breakage is manifested as an increase in electrical resistivity. Measurements to determine such consist of using two electrodes for current injection into the composite lamina and two electrodes to measure the drop in voltage between two points on the lamina. From this measurement, the resistance between the two points can be calculated. This technique, sometimes dubbed electrical impedance tomography (EIT), has also been demonstrated to be effective at detecting temperature changes in conductive materials, as this is another parameter that affects measured resistance/conductance (Chung 2001). One disadvantage of this technique, however, is that it has low zero-stability, meaning that over time the measurand will drift (Ko and Ni 2005).

The electrical resistance of carbon fiber-reinforced polymer (CFRP) composites is influenced by fiber breakage, delamination, mechanical strain, and temperature, and applications for SHM must take all these factors into account even if they are not of interest for SHM concerns. Anisotropic effects must also be considered, as in CFRP laminates the carbon fibers are oriented in a specific direction. In these materials it is well understood that the electrical resistance is low (~0.022 mΩ·m) in the direction parallel to the fibers and high (~310 mΩ·m) in the transverse direction (Angelidis et al. 2004).

Calculating the electrical resistance in unidirectional laminates (carbon fibers oriented in one direction) is thus straightforward. In multidirectional laminates, however, the situation is more complicated, and the arrangement of fibers in a network must be considered. Angelidis et al. (2004) compared the electrical resistivity of unidirectional, cross-ply (two orthogonal fiber directions), and quasi-isotropic (two pairs of orthogonal fiber directions) CFRP laminates. Sample specimens were 60% fiber by volume, 2 mm thick, and 30 mm² in area. EIT with four or two contact points was used for resistance measurements. They were able to demonstrate that, for unidirectional laminates and homogeneous current injection (achievement of which is described in the paper), resistance increases with positive strain in the lateral direction due to shrinking fiber diameter and in the transverse direction due to decreasing fiber contacts.

Wen and Chung (2000) demonstrated the use of electrical resistance measurements in measuring relative strain and the identifying damage under dynamic loading conditions. They employed EIT using silver paint and copper wire on the surfaces of plain cement, silica-fume cement, and latex cement pastes. They were able to observe changes in electrical resistance indicating both destructive plastic deformation as well as healing (e.g. closure of microcracks) in real-time. EIT was utilized by Schueler et al. (2001) in damage detection for CFRP composites with a resolution of 5 mm on a 50 mm by 50 mm grid with 1-mm spacing.

Song et al. (2006) demonstrated a revolutionary concept of a self-monitoring, self-healing concrete building. The building featured shape-memory alloys (SMAs), specifically martensite Nitinol cables, as reinforcement. When the SMA cables are resistively heated, they contract and close the cracks. Damage detection was accomplished with lead-zircontate-titanate (PZT) piezoelectric wafers which also estimated crack width based on the electrical resistance change in the SMA cables. Their concept was proofed with an SMA-reinforced concrete beam in which they produced a 0.47-inch wide crack under loading. They verified the monitoring and healing capabilities of their experimental setup and found that the electrical resistance value of an SMA cable changed by up to 27% in response to the opening crack.

Carbon nanotubes (CNTs) have also been studied in evaluations of the electrical resistance method of SHM. They are favored for their potential as actuators for high stress, high strain applications with low operating voltage. Due to their high tensile strength, they are also an attractive building material. The marriage of their architectural properties and their potential as stress/strain sensors presents a revolutionary potential for building self-monitoring ‘smart’ structures.

3.3 Electromechanical Impedance

Electromechanical impedance (EMI) typically takes advantage of piezoelectric materials, which produce an electric field when subjected to mechanical stress. The effect also works in reverse in that piezoelectric materials will produce stress and/or strain when in the presence of an electric field. Obviously, this makes such materials extremely valuable for the detection and monitoring of strain in structures as a single piezoelectric device can act as both source and receiver. What is particularly innovative about the use of piezoelectric materials is that the electrical impedance measured in the circuit is directly related to the mechanical impedance of the host structure (Park et al. 2000), which makes absolute measurement possible. Mechanical impedance is directly related to the fundamental characteristics of structures such as mass, stiffness, and damping—changes in which are indicators of structural damage (David et al. 2007).

A common EMI sensor is the piezoelectric wafer (patch), typically composed of piezoelectric-ceramic lead-zirconate-titanate (PZT), which is bonded to a structure or structural element to be monitored. By applying a voltage sweep signal—commonly in the kilohertz range—the PZT patch will induce vibrations in the structure. With an impedance analyzer connected to the wafer and controlling the voltage sweep signal, defects or deformations of the structure that are manifested as the electrical response of the PZT patch can be analyzed. By comparing conductance to frequency, a unique vibration signature of the structure is discovered which reveals structural characteristics like inherent stiffness, damping, and distribution of mass (Bhalla and Soh 2004).

Damage to the structure is especially apparent as changes in the structural stiffness and/or damping, so continuous monitoring that captures the dynamic behavior of the structure is most desirable. Such monitoring in real time can be achieved with the PZT wafer and numerous studies show how this sensor is successfully employed in permanent SHM networks (Lopes et al. 2000; Tanner et al. 2003; Lynch 2005; David et al. 2007). This method has been employed with great success and some studies have reported that it enabled the detection of cracks in concrete before they became visible, marking this technique as a clear improvement over standard, visual inspection methods.

3.4 Fiber Optics

Optical fibers are thin strands of dielectric material that trap light in a guided, low-velocity zone via total internal reflection, which is achieved by wrapping the waveguide or "core" in a "cladding"—a material with a lower refractive index. Optical fibers were first used for telecommunications and for endoscopy in medicine. By the late 1970's it was recognized that what distinguishes fiber optics best is that the materials are impervious to electromagnetic interference (Chang and Liu 2003) and so they began to be used as sensors; were also first used in concrete at the suggestion of Mendez et al. (1989). They are also attractive because they are lightweight and flexible, free from corrosion, allow for continuous monitoring, and possess very low signal transmission loss (Casas and Cruz 2003). Disadvantages presented by fiber optics are the cost and training required to decode optical signals.

One property of optical fiber that makes it ideal for use in SHM is that the light intensity of the optical signal decreases when the fiber is strained perpendicular to its length; light intensity can increase or decrease if the fiber is stretched or compressed (along its length). This enables fiber optics to be a valuable indicator of strain or displacement. To determine how much strain a fiber is experiencing, the signal's intensity is compared to that of an unstrained reference fiber of the same temperature. In the case of displacement, the change in length of the fiber can also be determined by measuring the light intensity and travel-time or “flight” time; this technique is called optical time-domain reflectometry (OTDR). These *intensity-modulated* sensing modes are examples of “intrinsic” properties of fiber optics—responses characterized by changes in the optical fibers themselves (Casas and Cruz 2003) and consequently the intensity, frequency, polarization, or phase of the signal (Merzbacher et al. 1996). This is the most common application of fiber optics to SHM, as the “extrinsic” case involves the use of fiber optics merely to convey an externally-generated signal (i.e. a signal from a computer or another sensor). Succinctly, extrinsic properties are those exploited by an independent sensor or computer while intrinsic properties are exploited when fiber optics serve as the sensor(s) themselves.

Fiber optics, particularly fiber Bragg grating (FBG) sensors, are also used as *spectrometric* sensors, which obtain absolute measurements of frequency changes in the optical signal in order to assess mechanical or thermal strain of the fiber. FBGs are manufactured fiber-optic cables that have the property of reflecting a finite wavelength band and passing all others. As the spectral width in reflected wavelength of the FBG is typically much smaller than the band of white light used in fiber optics, multiple Bragg gratings can be installed on the same fiber—a technique called *multiplexing* which allows the profiling of multiple parameters throughout a structure in real time on the same length of fiber cable (Chang and Liu 2003). Fiber-optic sensors without multiplexing are said to be *distributed* if they report conditions averaged along their entire length (i.e. if external forces along their length affect the signal) or *localized* if they report conditions only at a specific segment in the fiber (Lau 2003).

The advantages of absolute rather than relative measurement, wavelength-encoding, and an increased life span without calibration make spectrometric sensing preferable to intensity-modulated sensing. FBGs are sensitive to temperature and strain, however, the effects of which must be considered when using them to monitor any other parameters. Even when the desired measurement is strain, the strain of the structural member that is being monitored—both the load and thermal components—must be separated from the change in the optical properties of the fiber.

FBGs have also been used as inclinometers as they offer higher accuracy than other techniques and also possess the capability of multiplexing. In such applications, the temperature-dependence of strain is compensated for by having two distinct FBG sensors, for which dissimilar shifts in wavelength would be indicative of a change in the cable’s inclination while identical shifts are known to be the product of temperature change (Casas and Cruz 2003) and can be ignored.

A third kind of fiber-optic sensor, *interferometric*, is also useful for monitoring strain and temperature variation. Most interferometers consist of two fiber wires—one acts as a reference wire—so that the signals can be compared. Various kinds of interferometric fiber-optic sensors have been demonstrated including the common Mach-Zender configuration, the Michelson interferometer (based on the famous Michelson-Morley experiment), and the Fabry-Perot configuration, which unlike the others consists of only one fiber wire manipulated in such a way so as to form two parallel reflectors. Though early interferometric fiber-optic sensors were too slow for dynamic or continuous measuring, later developments enabled their signals to be demodulated at frequencies of up to 1 kHz (Inaudi and Glisic 2004).

Fiber-optic sensors of all kinds (spectrometric, interferometric, and intensity-modulated) can also be used in crack and displacement detection, which is otherwise performed through time-consuming and subjective visual inspection. Interferometric sensors sometimes operate as acoustic sensors—detecting the immediate development of a crack by the air wave it produces, which modulates the phase of the optical signal; this is described most notably by Ansari (2005). Most fiber-optic sensors used for this detection are interrogated with OTDR but the deployment of the sensors varies widely. The most successful application of fiber-optic sensors for crack detection involves embedding the sensors in a “zigzag” shape. With the knowledge of where kinks in the fiber were placed, comparison of light intensity before a crack occurs and after a crack occurs can yield information about the location of the crack. The disadvantage of this method is that it requires an assumption about the direction of cracks (that will develop) in the structure to ensure that the kinked fiber-optic cables are aligned correctly. Similar success has been achieved in the realm of monitoring existing cracks as they develop and the associated change in load on structural elements (Kuang et al. 2003).

Other applications of fiber-optic sensors have been explored that lie outside the field of SHM but some are directly relevant. FBGs have been used simultaneously as a corrosion transducer and temperature sensor simply by adding a metal coating to one segment of the fiber (Lo and Xiao 1998). Others have reported on using FBGs as accelerometers in a spring-mass system not dissimilar to a seismometer (Krammer et al. 2000). Still other applications include using FBGs as load cells and for traffic monitoring and ice detection on decks (Casas and Cruz 2003) as well as pH-sensitive corrosion detection (Panova et al. 1997) and delamination identification (Ling et al. 2005).

In conclusion, fiber-optic sensors are ideal for the SHM of reinforced concrete because they are stable, either localized or distributed, possess adequate sensitivity and dynamic range, provide linear response, are sensitive to the direction of a measured parameter’s change, are single-ended (minimal leads), insensitive to electromagnetic disturbance, capable of absolute measurement, nonperturbative to the structure, able to multiplex, easy to mass produce, and match the lifetime of the structure. Among the different types of fiber-optic sensors available, fiber Bragg grating sensors have the most distinct advantages in that they are intrinsic, have a linear response and require no calibration (Merzbacher et al. 1996).

3.5 GPS and Geodetic Measurements

Global positioning systems (GPS) offer an opportunity to make absolute displacement measurements of structures and structural elements in real time using the known positions of Department of Defense (DOD) satellites and the travel time of electromagnetic signals between them and the target. Due to the great distance of these satellites and, consequently, the great path length their signals travel through, GPS has, for much of its history, been unable to provide the necessary resolution for SHM, even after the policy of intentionally degrading the signals (for national security purposes) was lifted (Kijewski-Correa 2005). However, innovative signal processing techniques have enabled civilian users of GPS to obtain the resolution required for multiple applications including SHM.

For instance, although the ionosphere contributes significant time delay to these GPS signals, it does so at a rate proportional to their frequency. Therefore, estimates of this added delay can be made by comparing the arrival times of two signals of different frequencies—standardized as L1 (1.57542 GHz) and L2 (1.22760 GHz)—the latter of which can only be received by GPS units that are dubbed *dual frequency receivers*; others receive only one frequency (L1). Differential GPS (DGPS) further enables the user to correct for local environmental effects such as temperature and humidity by comparing signals of interest to those received at a reference station. The overall accuracy of such corrections is obviously proportional to the baseline separation between the target and the reference (Kijewski-Correa 2005). None of these corrections are able to overcome *multipathing*, however, where GPS signal reflections arrive later than the original signal—a phenomenon similar to "ghost" images on television screens and the ability to hear one's own voice as feedback on a cellular telephone call. The multipath effect can be avoided, however, through the use of a specialized "choke-ring" antenna that significantly reduces the strength of incoming signals, thereby preventing re-radiation of GPS signals (Huynh and Cheng 2000).

The accuracy attainable with these corrective procedures in place is within a few millimeters in near real-time (Knecht and Manetti 2001). One such system developed for SHM, described by Knecht and Manetti (2001) has as its goal a modular architecture, connectivity via the internet, and ease of installation, configuration and maintenance while the sensors themselves where desired to be of compact size, resistant to adverse environmental conditions, self-powered, and maintenance-free. The system consisted of mobile GPS receivers placed directly on the target object and a couple of reference receivers, identical to those installed directly on the target, which were placed at nearby locations, sometimes surveyed. The system demonstrated the capability of wireless link via radio or cellular modem. Solar panels and intelligent power-supply management of batteries provided the autonomous power required. All units communicated with a base station responsible for both data collection and processing and which also enabled remote access and configuration via a web browser. Ultimately, decisions and alerts based on measured positions and displacements were automated by the base station.

Meng et al. (2007) demonstrated a technique for measuring bridge deflection and peak dynamic character by combining a GPS antenna and a triaxial accelerometer. The accelerometer was driven by time pulses from the GPS antenna at a rate of 1 Hz in order to synchronize its measurements with that of the GPS unit. A band-pass filter and fast Fourier transform (FFT) were used to precisely determine local, dominant frequencies. These determinations were compared to the predictions of a finite element (FE) model for the Wilford Bridge, a suspension footbridge. For example, they determined that dominant frequency over whole band is 1.732 Hz compared to the FE model's prediction of 1.740 Hz, the first natural frequency. They demonstrated an ability to extract structural modal parameters such as natural frequencies, mode shapes, and damping ratios from the GPS and accelerometer measurements of ambient vibrations.

3.6 Magnetic and Magneto-Elastic

The magnetic flux leakage (MFL) technique is used for the detection of flaws in small-diameter bridge hanger cables. This technique requires that the target under inspection be placed in or subjected to a homogeneous magnetic induction field in which the main axis of the field is along the cable's length. Any flaw such as a broken wire in the cable will be manifested as a perturbation of the magnetic field—or what is termed a *magnetic flux leakage*. The intensity of this leakage is determined by the size and position of the flaw. MFL requires an in-situ sensor system that travels along the length of the cable and requires anywhere from 10-20 minutes per cable to an entire day per cable. This technique is far from favorable due to the time required for completion, the heavy amount of preparation of cable surfaces, and the bulk and cost of equipment (Mehrabi 2006).

Elasto-magnetic technology is an innovative approach to measuring the strain within bridge cables. The technique is based on the magnetic properties of ferromagnetic materials. The conventional picture of these materials in the demagnetized state is that they are made up of a myriad of magnetic "domains" each magnetized to saturation but possessing a random magnetization vector. The superposition of all of these random magnetization vectors results in a net magnetization of zero. In most scenarios, it is the application of an external magnetic field that changes the configuration of these domains by the movement of domain walls. However, mechanical stresses are also capable of moving domain walls and thereby stimulating the intrinsic magnetic field. By exploiting this relationship, the stresses that ferromagnetic materials are subjected to can be measured. An elasto-magnetic sensor, as proposed by Sumitro et al. (2002), consists of a hollow cylinder through which a steel (or other ferromagnetic material) structural element passes through. Ideally, this sensor should be installed during the construction.

The sensor itself contains primary, secondary, and compensating coils sealed with an insulating material. The life of this sensor is estimated to be no less than 50 years; it is weather-resistant and mechanically decoupled from the structural element.

The magnetic properties of steel are sensitive to temperature variations (on the order of 0.01 Wb/C), and careful correction for temperature changes is required while correlating magnetic field measurements to stress variations and corrosion in steel elements. Singh et al. (2004) attempted to detect corrosion of steel members by measuring the voltage induced in a conducting coil. Corrosion can be inferred from a change in cross-sectional area which is equal to the rate of change of magnetic flux. The rate of change of magnetic flux, in turn, is responsible for voltage induction in the coil. They calibrated their observations by varying the temperature of a sample through resistive heating and measuring magnetic flux every 5°C increase. The experimental setup was used for steel bars with varying mass% loss due to corrosion. They demonstrated how field measurements of steel elements can be compared to identical, non-corroded reference steel in order to quantify the amount of corrosion present.

Another magnetic technique applied to SHM is the use of a Superconducting Quantum Interference Device (SQUID). A SQUID is a highly sensitive magnetic flux-to-voltage transducer—it senses minute changes in magnetic flux and reports them by voltage changes. Advantages of SQUID as a measurement system include its high sensitivity (~10-100 fT $Hz^{-1/2}$), wide bandwidth, and broad dynamic range (>80 dB). In addition, as SQUIDs function at zero frequency they are able to achieve greater depth penetration than eddy-current sensors, as capable of detecting and monitoring the flow of steady-state corrosion currents, and can image static magnetization of paramagnetic materials (Jenks et al. 1997).

SQUIDs achieve their high sensitivity by utilizing superconducting materials. These materials, when cooled below a certain critical temperature T_C, exhibit zero resistance—hence, they are “super-conducting” in that they allow current to persist indefinitely within them without any external power supply. SQUIDs are classified by the material that makes up their superconducting element, and these fall into two classes: superconductors with a high T_C and those with a low T_C. Both are used in SQUIDs but high-TC superconductors are favored because it is less difficult to reach their critical temperature. The cooling of high-T_C materials is often accomplished with liquid nitrogen, which is commonly available, easy to handle, and cheap compared to liquid helium—the staple for low-T_C superconductors. However, the best signal-to-noise ratio for SQUIDs is achieved with low-T_C superconductors, and they currently dominate the practice (Jenks et al. 1997).

Another curious property of superconducting materials is that they expel any internal magnetic fields—a phenomenon known as the Meissner effect—which means superconductors possess no internal magnetic fields. When superconductors are shaped into a loop or are embedded so as to surround non-superconducting materials, however, they demonstrate yet another curious property: the quantization of magnetic flux. In all superconductors, regardless of their constituent materials, supercurrents (electrical currents that arise in superconductors) are arranged at the material boundaries in a way so that the induced magnetic flux is a multiple of the flux quantum. Furthermore, these supercurrents oppose any change in flux that may be applied to the superconducting loop.

The quantization of magnetic flux is what enables the SQUID to operate. As the supercurrents oppose any change in magnetic flux, such a change would be marked by a change in current flow across the superconductor. This results in a phase change, which can be detected in a Josephson junction—a pair of superconductors weakly connected across a junction of insulating material. SQUIDs are capable of making sensitive measurements of magnetic flux because they consist of one or two Josephson junctions.

In all SHM applications of SQUID, measurement begins with the imaging of the magnetic field distribution in the vicinity of the target. This is done either by monitoring intrinsic currents (e.g. galvanic currents in a corroded specimen) or external sources. The latter technique requires direct contact with the target when electrical excitation is used, however, excitation can be achieved without contact if a strong magnetic field is applied. Jenks et al. (1997) postulate that damage or failure prediction in steel elements may be possible with SQUIDs. They cite studies in which SQUIDs have been used for the detection of flaws in steel plates where a magnetic field was induced by a superconducting solenoid. Such a study found that machined voids as small as 2 by 1 mm^2 could be detected at a stand-off distance of 4.2 cm. They cite a more realistic study by Cochran et al. (1993) in which fatigue cracks in 12.5 mm-thick steel plates were identified. Krause et al. (2002) used four SQUIDs in conjunction with four Hall probes and four magnetoresistive sensors to detect breaks in reinforcing steel of a concrete bridge and were able to locate such defects to within ±5 cm. Applications of this technology for composite materials are described in Section 6.1 Fiber-Reinforced Polymer Composites.

3.7 Ultrasonic Emissions and Lamb Waves

Ultrasonic acoustic emission monitoring (ultrasonic AEM) is one of the most commonly used inspection techniques for steel structures. As with electromechanical impedance monitoring (described in Section 3.3 Electromechanical Impedance), an acoustic signal is induced in the structure from which reflections are interpreted in the search for defects (Chang and Liu 2003). More specific information about impedance monitoring can be found in Section 3.3 Electromechanical Impedance. The principle is the same in traditional SHM techniques like chain dragging and the tap test. Aside from the oftmentioned subjectivity of these traditional techniques, they are also limited to audible frequencies.

The distinct advantage of ultrasonic waves (generally, frequencies higher than 30 kHz) is due to the acoustoelastic effect, in which stress causes a change in ultrasonic wave velocity (ultrasonic pulse velocity or UPV). UPV techniques are affected by the inherent properties of the concrete, however, in addition to internal stresses; considerable computation time to address this complexity is required for most applications. Other modes of analysis, such as ultrasonic wave attenuation, are known to be indicators of microstructural features of interest, but there is a lack of consensus as to how the parameters should be measured.

In concrete, the impact-echo method has been employed with success in flaw detection. The method is based on the study of reflected stress waves that change in frequency character when transmitted through flawed material. It has been demonstrated to be effective in the detection of delamination, voids, and honeycombing (Chang and Liu 2003). At the forefront of AEM techniques are non-contact methods employing directional microphones, however, this method of noise reduction is ineffective at high noise levels or in complex sound fields (Zhang et al. 2010). The ambient noise that plagues acoustic evaluation is commonly encountered in the field where these techniques are applied on busy roads or highways.

Zhang et al. (2010) attempted to improve upon the problems that exist with AEM. They sought to address ambient noise by applying a modified independent component analysis (ICA) technique used to separate sounding (impact) signals from noisy recordings. They also eliminated subjectivity through the use of mel-frequency cepstral coefficients (MFCCs) for automatic detection—MFCCs are often used in acoustic signal processing for other applications. They were able to demonstrate high detection accuracy using MFCCs and a mutual information maximization algorithm. Though the performance decreased with increasing noise, they managed to compensate and improve detection at high noise levels with the modified ICA.

Global acoustic techniques typically involve spectral or time-domain analyses. These allow for feature extraction, frequency determination, and the vibration or displacement of structural elements. These can be determined from three distinct types of spectral analysis: Fourier, wavelet, and Hilbert-Huang transforms (HHT).

Lamb waves are a special case of elastic waves. As with electromechanical impedance techniques they are generated by piezoelectric transducers for the purpose structural health monitoring. Lamb waves are guided elastic waves whose particle motion occurs along the surface of a material in a plane described by the normal to the surface and the direction of propagation. They occur in materials with a uniform thickness on the order of a few wavelengths. They are in fact identical to Rayleigh waves in earthquake seismology—which propagate along the Earth's crust—with the exception that Lamb waves are guided waves. Due to their relatively short wavelengths, they have shown promise in detecting highly localized defects (Crider 2007).

The methods commonly used for Lamb wave detection are *pitch-catch* and *pulse-echo*. The pitch-catch method uses two transducers—one for excitation and the other to receive signals—where damage is interpreted from the change in response. This is a global method where an insufficient number of transducer pairs are used, but can be deployed so as to locate damage specifically. The pulse-echo method uses only one transducer which acts both as source and receiver. The single transducer detects returns (echoes) from which the location of material defects can be inferred from the travel-time and the severity of damage from the amplitude of the reflection.

4.0 On-Site Monitoring Techniques

4.1 Eddy Currents

Eddy detection is conducted by the use of a probe coil—which may have either an empty, air core or a magnetic ferrite core—that induces electromagnetic currents in conducting materials. These currents nominally radiate from the coil in circular patterns (eddies). In the presence of a flaw in the material, however, these current patterns are disturbed at the site of the flaw, such as a crack. Although widely used in the inspection of surface and subsurface cracks as described, this technique requires the use of a differential probe when applied to weld metal due to the wide variation in magnetic material properties. The technique remains effective even when applied to surfaces with nonconductive coatings such as zinc-based primers and lead paint (Chang and Liu 2003).

The meandering winding magnetometer (MWM) is a special type of eddy current sensor that features a meandering primary coil for induction and numerous fully parallel, secondary coils for sensing. They are typically deployed in scanning arrays but are also used for a wide variety of applications in permanently-mounted arrays. MWM arrays are particularly well-suited for fatigue monitoring. In such an array, a drive winding, made up of linear drive segments, is stimulated by a current at anywhere from 1 kHz to 40 MHz to produce a time-varying magnetic field capable of inducing eddy currents in the pattern of the drive winding. MWM arrays achieve high resolution, usually down to 1 mm by 1 mm surface areas, with the use of numerous, tiny sensing coils (Zilberstein et al. 2003). Usually, these are adhered to a substrate allowing for the production of thin and flexible ‘chips’ that serve as sensors. Their size and flexibility allows them to be permanently attached to or embedded in the element to be monitored under real load conditions. Micromachining enables the production of these chips so they are cheap and identical to one another.

Zilbertstein et al. (2003) describe the processing of MWM array data by inversion of the measurement grid, which converts sensor impedance magnitude and phase response into material properties such as electrical conductivity or magnetic permeability. They ran several cyclic loading tests on plain shot-peened plates and combination shot-peened-cadmium plates, letting some of the fatigue tests run to failure while others were terminated according to when the MWM array measurements of magnetic permeability indicated the onset of failure. Fatigue and cracks were identified using scanning electron microscopy (SEM). They surmised that gradual increases in magnetic permeability corresponded with fatigue damage prior to the formation of cracks that are much shorter than the grain size. They were able to detect the formation of cracks on the order of 250 μm or less in length. This capability has been previously demonstrated for aluminum alloys.

4.2 Electrical Time-Domain Reflectometry (TDR)

Bridge scour is a potentially devastating condition in which the adjacent and underlying sediments of bridge piers and abutments are removed due to erosion and related stream processes. The current method of predicting or assessing bridge scour relies on empirical scour prediction equations that have been generated from laboratory data. These equations generally do not adequately predict actual scour in the field, however (Yu and Yu 2009). Some field monitoring techniques have been developed from the use of a simple yardstick to more advanced methods such as ground-penetrating radar (GPR) and ultrasonic techniques. These methods do not allow for real-time monitoring, however, nor are they sufficiently rugged or automated.

Yu and Yu (2009) propose time-domain reflectometry (TDR) as an improvement over the current methods of predicting bridge scour. TDR has been used in other studies to the same end but the technique employed by Yu and Yu (2009) improves upon all of these earlier attempts and is capable of predicting scour depth, the density of sediment materials, and the electrical conductivity of river water.

TDR was first used by electrical engineers to locate discontinuities in electrical power and communication lines. It also provides a way of measuring the dielectric and electrical properties of materials. Specialized TDR devices that serve as pulse generator and sampler are used to send a fast-rising step pulse or impulse to the sensor probe. The TDR device measures the reflections due to either the change of system geometry or material dielectric permittivity. TDR is effective at discerning the sediment geometry and diagnosing bridge scour because of the large contrast in dielectric constant between water and air or sediment solids. These contrasts cause large reflections at the interfaces where they exist, such as the air-water boundary and material layers.

A real-time TDR scour-monitoring system consists of TDR probes permanently installed at the base of bridge piers and abutments. From the measurements made with these devices and the automated signal processing developed by Yu and Yu (2009), when scour depth exceeds the bottom of the structural element, a warning can be issued to bridge managers, allowing them to implement appropriate countermeasures to prevent catastrophic failure. There are some potential anomalies that have to be taken into consideration, however. Turbulent flow during storm or flood events, for instance, will affect the scour signal.

4.3 Infrared Thermography and Spectroscopy

Infrared thermography is the detection of electromagnetic waves in the infrared spectrum. More specifically, it is the detection of the strength and location of thermal anomalies and in the context of SHM these anomalies are (ideally) structural defects. This technique is commonly applied directly to concrete and asphalt decks for the detection of thermal variances that are given by radiation, conduction, and convection (Maser and Roddis 1990). Infrared thermography has found favor in the SHM of transportation infrastructure because it requires shorter inspection time than many other methods which directly results in fewer or shorter traffic lane closures. Infrared thermography differs from infrared spectroscopy in that the spectrum of infrared radiation (the range of frequencies and their respective amplitudes) is only of significance in the latter.

Thermography is commonly used for the detection of concrete or asphalt delaminations, as surfaces with such underlying defects lack contact with bottom material that would otherwise act as a heat sink. Consequently, these delaminated areas will be warmer with respect to adjacent, full-bonded areas. A homogeneous material such as concrete cools quickly when it is warmer than its environment (e.g. after sunset). As it cools, the top surface of the concrete draws heat from lower layers. Defect areas, however, prevent or reduce this heat transfer and, as a result, surface areas above them cool more rapidly than surrounding areas. Conversely, when concrete is cooler than its environment, these surface areas warm at a slower rate than their surroundings (Howard et al. 2010). Passive thermography (i.e. the use of solar heating) has been described in the available literature as well as an active technique in which radiative heaters are used to heat (or cool) the target before infrared images are collected; both techniques are usually non-contact techniques (Alqennah 2000). Examples of radiation sources (and sinks) are hot air guns, quartz lamps, xenon flash lamps, hot (or cold) water, vortex tubes, and liquid nitrogen (Burleigh and Bohner 1999). As environmental conditions such as insolation (input solar radiation) and air temperature vary throughout the day, the thermal behavior of a concrete deck also fluctuates diurnally and thus requires compensation for these external factors.

A more complete list of factors influencing the thermal emission of a concrete deck includes: the deck’s characteristic emissivity, deck surface temperature, ambient air temperature, deck thermal conductivity, deck volumetric heat, the thickness of the heated layer, solar radiation intensity, and air velocity (Maser and Roddis 1990). Thus, a simplified model of the physical system can be very useful for interpreting deck conditions. Maser and Roddis (1990) propose a model driven by an insolation function and ambient temperature. Between the concrete deck and the air temperature, some heat flux terms are linear (conduction) while others are non-linear (convection and radiation). For simplicity, they combine all three heat fluxes using the concept of a heat transfer coefficient. This linear approximation is valid to within ±5% for most cases. Their model included such physical approximations as modeling delamination by an air-filled crack, and this agreed with ground-truth data. Changes in the dimensions of this crack had a corresponding effect on the temperature difference observed. A much smaller difference in temperature between the solid deck and a water-filled crack was observed, as the thermal conductivity of water is not substantially lower than that of concrete. In a similar study using this model, Maser and Roddis (1990) identified certain conditions (e.g. thick asphalt, small delamination width) under which the thermal anomalies are too small to detect. Alqennah (2000) reports that the method is insensitive to delaminations at deeper than half the thickness of the deck. This is consistent with the findings of another report by Howard et al. (2010).

During loading, a concrete deck may exhibit several thermo-mechanical effects—responses of a material's thermal properties to mechanical loading. Thermo-elasticity, heat dissipation by reversible anelastic dampening or by irreversible plastic deformation, and surface friction are all factors in temperature change during cyclical loading. Meyendorf et al. (2002) investigated the thermo-mechanical effects of loading and their applications to fatigue characterization. They measured the aforementioned thermo-mechanical effects as a function of accumulated fatigue cycles during interrupted fatigue tests conducted on cylindrical dog-bone specimens of machined titanium with 6% aluminum and 4% vanadium by weight. Thermal excitation was achieved, following fatigue loading, by high-frequency ultrasonic waves and low-frequency mechanical loading, alternately. They demonstrated that the temperature change per cycle ($\Delta\tau_{diss}$) is exceptionally sensitive to fatigue damage in its early stages. They also concluded that microstructural variations caused by fatigue could be identified by determining the dissipated heat per loading cycle.

Detection and quantification of chloride intrusion is one of the more difficult challenges for NDE as it is manifests as a regional, chemical property of the affected concrete structure. Infrared spectroscopy, however, has been used with success to identify chloride intrusion and evaluate chloride content (Kanada et al.). Such an application takes advantage of the fact that absorbance of thermal radiation increases with chloride content at a peak wavelength of 2266 nm. Kanada et al. found a correlation between difference spectra and chloride content as high as $R^2=0.99$. In their experiment, controls consisting of concrete cores with various, known chloride content were used to calibrate a field detection scheme. In a separate experiment, they extended this technique to the detection of carbonation and sulfate attack.

Alqennah (2000) reports on multiple thermography techniques that have been employed by others. (Winfree 1998) found that tailoring the shape of radiative heating can improve the sensitivity in detecting deep delaminations. Thermal inertia mapping is a thermography technique that measures the resistance of a material to temperature change, which is achieved by determining the inverse slope of the surface temperature versus the inverse square root of time. This technique was employed by (DelGrande and Durbin 1999) to detect delamination in reinforced concrete structures, and has also been successfully used to detect airframe material loss due to corrosion. They demonstrated that the technique can determine the fractional area of delamination and can be applied to "cluttered" (debris-strewn) concrete decks if a flash-heated stationary system is used.

Alqennah (2000) writes that while thermography has been useful in the detection of concrete deck conditions it has not yet been applied successfully to structures of composite materials. However, that account predates the reports of others who have used it to successfully detect damage in FRP composite structures (Bates et al. 2000; Hu et al. 2002; Meola et al. 2004; Halabe et al. 2005). For more information on such studies, consult Rao (2007) or Section 6.1 Fiber-Reinforced Polymer Composites in this paper.

Howard et al. (2010) describe the development of a commercial infrared imaging system for detecting concrete bridge deck delaminations. *BridgeGuard* rapidly evaluates deck conditions at typical driving speeds, immediately analyzing and storing the data within a data management system for future reference. The authors report that there are two ideal 'windows' for infrared imaging, one beginning a few hours after sunset and the other beginning a few hours after sunrise. At these times, when skies are clear, the thermal properties of concrete can be exploited for maximum efficacy. In their initial report they found that 1600 hours offered maximum solar contrast while 0300 hours offered maximum non-solar contrast.

4.4 Laser Scanning

Terrestrial laser scanning (TLS) refers to the practice of illuminating target objects and structures with a ground-based (hence 'terrestrial') laser. Airborne laser scanning (ALS) refers to the same when it is conducted by an airborne platform. Both are methods of light detection and ranging (LiDAR) and are used for the purpose of either detection and ranging or measurement of displacement and velocity. The common method of achieving the latter objective is through interferometry. Both TLS and ALS are discussed here.

The advantages of TLS lie in its ability to reach structures of any size or any structural members, the lack of dependence on natural light sources or supplementary illumination of the target, and that no wiring or in-situ sensors are required to be installed or maintained. As with ALS, the principle of 3D coordinate extraction is based on the travel-time of a pulse of light transmitted between instrument and a point on the structure or structural member of interest. By combining this information with the laser's rotation angle (both vertical and horizontal), coordinates are obtained without the need of any computational post-processing—they are obtained as absolute measurements from the emission of 10^2-10^6 laser pulses (Park et al. 2007).

Another boast of TLS and other laser scanning techniques is that they provide coordinate information in terms of the absolute position of the target (rather than relative deflections). Achieving this is not so straightforward, however. It requires the transformation from the TLS coordinate system into the structural coordinate system by calculating *base vectors* which represent the distance to the target.

Commonly, laser scanning systems in SHM are used for the detection of shape changes or displacements. (Liu et al. 2010) have demonstrated that laser scanning is also capable of clearance detection, bridge load testing, and construction monitoring. In order to determine displacements or shape distortions of structural members with TLS, it is necessary to scan the target multiple times, ideally once before the structure is loaded or stressed and then at least once afterwards. In this fashion, the differences between the scans correspond to deformations or displacements of the structure. As with other innovative techniques for obtaining these measurements, results have been compared to those of established detection methods such as the use of linear variable displacement transducers (LVDTs) or accelerometers.

LiDAR usually refers to ALS exclusively rather than to both terrestrial and airborne methods. It is a popular technique in the fields of GIS and remote sensing as it allows three-dimensional location information of an entire object. Since its inception it has been used in these fields primarily to acquire topographic information, particular in the production of digital terrain models. When applied to SHM, LiDAR allows the measurement of displacement in three dimensions as well as shape deformation of specific structural elements. As a “stand-off” method of monitoring, LiDAR has the advantage of not requiring any sensors, wiring, or supplementary illumination.

LiDAR operates in a similar fashion to radar, hence the similarity in the naming convention. LiDAR is more straightforward and enjoys more simplicity, however, in that the principle of three-dimensional coordinate extraction using LiDAR is based solely on travel time between the source of the laser pulse and the target object. High accuracy requires that the laser source be closer to the target object than other remote sensing modules (such as radar satellites), however. In general, for all laser scanning the source should not be farther than 350 m from a target with minimum reflectivity of 4% (Park et al. 2007). One study cites horizontal and vertical position errors of about 10 mm with distance errors of no more than 7 mm at a distance of 100 m from the target object (Lee et al. 2005). Errors were further reduced in this study by the application of the least squares method following coordinate transformation. Rice et al. (2010) report accuracy within 1 mm at a maximum range of 200 ft.

One important objective of LiDAR, be it terrestrial or airborne, is to determine the dynamic character of a structure. As such, ambient vibration methods have been investigated as a means of quantifying the elastic properties of buildings and evaluating the performance of structural retrofits. Although most ambient vibration surveys are conducted with accelerometers or velocimeters, Gueguen et al. (2009) argues that there is much to be gained from performing these surveys remotely (with LiDAR). They cite the ease in performing the survey without applying instruments directly to the structure and the increased safety of assessing ambient vibrations remotely in the case of seismological hazards, particularly when aftershocks are expected. In their paper, they describe an experiment that compares the ambient vibration measurements of conventional, in-situ sensors with that of coherent LiDAR.

Coherent LiDAR exploits the Doppler effect to make precise measurements of micrometric vibrations over great distances. When illuminating a moving target with a laser source, the backscattered signal is shifted in frequency proportional to the difference in velocity between the target and the LiDAR platform. If the vibration of the LiDAR platform is separated out, the motion of the target can be effectively quantified. For simplicity, Gueguen et al. (2009) performed their experiment with the LiDAR platform inside the subject building with the instrument pointed at the ground. This way, the illuminated target was known to be stationary as opposed to if the building was illuminated from the ground. It is valid to assume that the same measurements will be obtained provided that there is no structural variability during the normal period. After comparing the LiDAR measurements to those of the in-situ velocimeter, they concluded that although the signal-to-noise ratio was lower for LiDAR, the techniques compared very well.

4.5 Nuclear Magnetic Resonance (NMR) Imaging

Nuclear magnetic resonance (NMR) is a phenomenon in which certain atomic nuclei in static magnetic fields, when exposed to oscillating electromagnetic (EM) radiation, absorb and re-radiate the energy at specific resonance frequencies. It is commonly applied in magnetic resonance imaging (MRI) to generate detailed images of biological tissues. The human body is composed mostly of water molecules and this is why MRI is such a successful investigative technique. Sensitivity to water is exactly why the technique has been adopted in SHM as well, though with some modifications.

Hydration is a key concern in concrete durability and tensile strength. Chloride ingress and corrosion of steel reinforcement are obvious consequences, however, there is also a danger of explosive spalling during fire with high moisture content. The inverse relationship between tensile strength and the water-to-cement ratio of concrete is well established. Compressive strength, too, is adversely affected by high water content (Li 2004). Porous concrete in northern climates is especially vulnerable to frost-wedging and other freeze-thaw degradation as water alternately freezes (and expands) or thaws (and contracts). Water content of cement paste is also a concern as concrete strength deteriorates due to the contraction associated with freeze-thaw events and other volumetric changes that exert pressure on pore walls. Excessive drying will also lead to shrinkage and subsequent cracking due to stress at the aggregate-paste interfaces. It has been reported that moist curing followed by drying to a moisture content of less than 90% relative humidity boosts concrete's freeze-thaw resistance (Beyea et al. 1998).

The relaxation rate (how fast the nucleus' magnetic vector aligns with the main magnetic field initially or following tilt by radio-frequency pulse) of hydrogen atoms is often measured in NMR experiments, as it is strongly dependent on their mobility. This allows scientists to distinguish between frozen and non-frozen water, as one example. The spatial distribution of moisture content in concrete is determined by drying mechanisms, capillary flow, and molecular diffusion (provided the concrete is exposed to air). Careful application of MRI has allowed for the quantification of non-frozen water distribution in concrete samples. It has also been demonstrated that this technique could be applied under a variety of real weather conditions (Prado et al. 1997). It should be mentioned as a distinction from other SHM techniques described in this paper that NMR as described in the literature today is actually a destructive technique that admits only small samples taken from existing structures.

After hydrogen ^{1}H (because of its presence in water molecules), the most important nuclei for cement and concrete research are carbon ^{13}C, aluminum ^{27}Al, and silicon ^{29}Si. Carbon ^{13}C is found only in small quantities in cement as it is often applied only as an additive. Its use in NMR is primarily centered on its ability to distinguish between plasticizers, which may be an indication of what deterioration the concrete has experienced. Aluminum ^{27}Al may also be useful for identifying the presence of fly ash and zeolites. Zeolites are also indicated by the presence of silicon ^{29}Si, from which information about silicate hydration can also be derived. In short, NMR may be useful in SHM for studying clinker composition, the hydration kinetics of cement minerals, the influence of admixtures, the reactivity of pozzolanic materials, binder structure and degredation, frost mechanism, cement-polymer interaction, and for macro-pore imaging (Justnes et al. 1990).

Both Beyea et al. (1998) and Prado et al. (1997) describe the use of single-point imaging (SPI)—a technique that uses phase encoding instead of frequency encoding in order to spatially image a sample. SPI improves upon MRI in concrete applications because the relaxation rate of water in concrete is typically much too small. SPI is effective because the relaxation time for water is known to decrease with concrete pore size. The technique has been reported to achieve sub-millimeter accuracy with an excellent signal-to-noise ratio. It has been used in drying experiments, to provide on-demand imaging of lightweight concrete, to study the freeze-thaw and salt ingress processes, and even for high-resolution, 3D imaging of water distribution in both porous and non-porous aggregates.

4.6 Microwave Radar

Radio detection and ranging (RADAR, but now almost exclusively "radar") is a well-established technique for measuring the range (distance to), altitude, direction, and speed of moving or stationary objects. This is achieved through the illumination and, commonly, the reflection off of an object with electromagnetic (EM) waves. Reflected EM waves are detected at the transmitter, making it both source and receiver. Otherwise, separate transmitting and receiving probes are used in *through-transmission* techniques. In most civil engineering applications, the reflective technique is used as it requires only one surface be accessible (Bungey 2004). Microwave, millimeter, and radio wave inspection techniques typically operate at frequencies ranging from 300 MHz to 300 GHz in dielectric (electrically insulating) materials (Chang and Liu 2003). In order to achieve 3D displacement measurements, radar measurements from independent directions must be made, as radar can only measure displacement in the range direction, parallel to transmission (Pieraccini et al. 2004). In the case of a fixed-position radar antenna, multiple targets at the same distance from the receiver (in the same *range resolution cell*) cannot be distinguished and are marked by one reflection for that *range bin*. Many of the principles discussed in this section hold true for all radar applications. In this paper, ground-penetrating radar (GPR) is discussed in Section 4.7 Ground-Penetrating Radar (GPR) while interferometric synthetic aperture radar (IfSAR) is discussed in Section 5.3 Interferometric Synthetic Aperture Radar (IfSAR).

Microwave and millimeter radar techniques first gained popularity in SHM because they offered more compact and less expensive equipment than GPR methods. Microwave radar is seen as a most promising SHM technique as it is able to penetrate deep inside concrete, attenuates much less due to scattering than acoustic methods, and offers excellent contrast between concrete and metal reinforcements. For concrete structures, the free-space reflection and transmission properties are a product of the material's behavior on the macroscopic level. Thus, they vary with the material's internal condition and superficial or deep elements of interest such as defects, reinforcement, moisture, and void spaces (Arunachalam et al. 2006).

There are many different techniques of operation for microwave radar in the near-field including diffraction tomography and open-ended waveguide measurements. These techniques require either direct contact or close-proximity to the target—generally much less than the transmission signal's wavelength—and, consequently, require some surface preparation or antenna positioning to avoid diffraction effects. The advantage of near-field techniques despite the rigors imposed by such requirements is their high sensitivity. Far-field techniques do not require such considerations and allow for a plane-wave assumption, which simplifies numerical models (Arunachalam et al. 2006).

Many microwave radar systems make use of a continuous-wave step-frequency (CW-SF) transceiver which emits continuous waves which step through discrete frequency values. CW-SF operation allows for the generation of deformation maps and the imaging of static displacements (Pieraccini et al. 2004). The use of CW-SF techniques imposes an upper limit on the range in which unambiguous range measurements can be made in accordance with the Nyquist-Shannon sampling theorem. Most development in this area has focused either on specific applications of CW-SF or making CW-SF systems respond fast enough for dynamic monitoring. In many radar applications, neural networks have great potential to automate the interpretation of results but, recently, success has been limited to simple cases such as the location of reinforcing bar (Bungey 2004).

4.7 Ground-Penetrating Radar (GPR)

GPR is the most commonly used radar technique in structural health monitoring. The technique is based on the emission of a very short time-duration (<1-20 ns) EM pulse in the frequency band of 10 MHz to 2.5 GHz; typically, no less than 500 MHz is used for practical applications. Antennae with a center frequency of a few hundred MHz or higher provide sufficiently high resolution detail of the shallow subsurface. However, as the Earth acts like a low-pass filter, these high-frequency antennae cannot penetrate farther than about 3 m depth. Penetration depth is achieved when the radar amplitude has been attenuated by a factor of e^{-1} though such a depth varies with attenuation factor and changes in the medium's electromagnetic properties. For deeper investigations, antennae with center frequencies below 100 MHz are used, though this sacrifices vertical resolution. 1 GHz antennae are well-suited for SHM goals such as crack detection, thickness estimation, and moisture detection (Arias et al. 2007).

Unlike other pulse radar systems that generate radio pulses at single, discrete frequencies, GPR operates in an "ultra-wide band" where radio energy is transmitted over a wide frequency band. In GPR, the EM signal is emitted continuously or in discrete repetitions as the antenna passes over the ground. These pulses are reflected by changes in the medium's magnetic permittivity, electrical conductivity, and dielectric permittivity. The receiving unit records reflected signals as changes in voltage as a function of time, thereby generating an image of the shallow subsurface (Arias et al. 2007). This 2-dimensional image is referred to as a *radargram* and consists of one axis corresponding to antennae displacement and the other corresponding to the two-way travel time of the pulse emitted. Just as in seismic surveys, the y-axis corresponding to travel time is a proxy for depth and the two are related by the velocity of the medium. This graphic display of radar data is the most common preparation for interpretation as it presents a cross-section of subsurface structure.

GPR surveys are conducted with either *air-coupled* or *ground-coupled* antennae. Air-coupled antennae are typically suspended at about 25 cm above the target surface which allows them to be safely operated at highway speeds when mounted to the back of a survey vehicle (Morey 1998). Air-coupled antennae have been employed successfully for rapid bridge monitoring. The technique has reportedly been used to survey 134 bridge decks in 32 days without any lane closures or traffic interference (Maser and Bernhardt 2000). Ground-coupled antennae cannot be used in such a survey since they require direct contact with the ground. The advantage of ground-coupled surveys, however, lies in their improved depth penetration. Both ground-coupled and air-coupled GPR surveys can be conducted on either bare concrete decks or concrete decks with an asphalt overlay.

The spatial (plan) resolution of GPR is determined by the antenna frequency, achieved depth, and the electromagnetic properties of the medium. Sensitivity studies have shown that the horizontal resolution of GPR can be as fine as 3-4 cm in a high-velocity medium such as saturated concrete (Perez-Gracia 2008). When there is only small spacing between anomalies, it can be difficult to discern buried objects from one another due to interference effects, which become significant at a spacing of less than 10 cm in lower-velocity media. However, even at a separation of 3 cm, the shape of the anomaly is usually enough indication that the source may in fact be two distinct objects. Effects of interference can be minimized through the use of Kirchhoff migration but this may not result in a corresponding increase in spatial resolution. Spatial resolution is maximized when the antennae are placed directly over and close to the investigative surface (Van der Kruk 2003).

Sometimes, multiple GPR reflections can lead to false indications of a boundary or transition. At all times, the strength and polarity of the reflection is determined by the contrast in the dielectric properties of materials at the interface (Bungey 2004). For concrete and asphalt applications, the parameter most strongly affecting the dielectric permittivity is moisture, making it easiest to detect and measure with GPR. Of course, as free moisture in concrete and asphalt is contributed to by the presence of chloride ions, it is also an effective method of monitoring chloride ion distribution. Responses from saturation and chloride ion content are both due to the polarizing effect of an electromagnetic field. Delamination is also consistently distinguished from solid concrete and asphalt (Maser and Roddis 1990). Pavement substructure characteristics such as material type, layer thickness, and variability have been determined with specialized signal processing of GPR data (Brooks et al. 2007). In such applications, GPR is a well-established technique; by the end of the last millennium, over 260 papers, patents, and standards had been published on the subject (Olhoeft and Smith 2000).

Pavement thickness is easily determined by measuring the time difference between layer reflections if the propagation velocity within these layers is known or can also be measured. Depth and spacing of dowels in jointed concrete as well as iron bars in reinforced concrete can be determined with radar tomography—one of the products of GPR. Scour refill in and around bridge supports and abutments can also be detected and its thickness quantified using GPR (Haeni et al. 1992). GPR has also been demonstrated as capable of detecting air- and water-filled voids with a threshold as small as 3 mm (Morey 1998).

In decreasing order of measurement reliability, the following is a list of some applications of GPR for structural concrete: thickness estimation from one surface, the location of reinforcing bars or other metallic objects, estimation of the depth of buried objects, location of moisture variations, location of voids, the dimensions of such voids, location of honeycombing or cracking, and an estimation of the size of reinforcing bars. Advantages of GPR are that it can rapidly and effectively investigate a large swath of one surface, it requires no coupling medium, it is continuous, results have a high potential to be improved through signal processing, and there are no special safety precautions required. Disadvantages include the requirement of highly specialized equipment, the need for calibration or 'ground truth' corroboration, the expense of equipment and signal processing, and the inability to penetrate metal features (Bungey 2004).

In a 1998 questionnaire, the Transportation Research Board (TRB) surveyed the use and familiarity with GPR of every state and territorial transportation agency in the U.S. and all of the Canadian transportation agencies. From 51 responses, the TRB found that 33 agencies reported having some experience with GPR; 18 had no experience whatsoever with GPR. The most common applications of GPR employed by these agencies were pavement layer thickness (24 agencies), void detection (22 agencies), and bridge deck delamination (16 agencies). These agencies reported having been very successful in employing GPR for pavement layer thickness evaluation but reported less success using GPR in other applications (Morey 1998).

4.8 X-Ray, Gamma Ray, and Neutron Radiography

All radiographic techniques involve the use of a radiographic energy source on one side of an object and a sensitive film or other recording medium on the other side. Just as in medical or dental X-rays, the amount of radiation that impinges on the recording medium is determined by the density of the material it passes through. The result is a two-dimensional image of density variation within the structure, and while this technique has proved valuable in laboratories, it is not as viable for field use because the equipment is quite heavy and its power consumption large.

These devices commonly use either X-rays or gamma rays as the source and the techniques employed include measuring photoelectric absorption, Compton scattering of reflected gamma rays, and computational tomography (CT). CT requires the reposition of the radiographic source at multiple orientations so that a computer can construct a 3D image of the target (Chang and Liu 2003).

Alternatively, X-ray fluorescence is a technique in which source and detector are on the same side of a target surface. The principle of X-ray fluorescence is exploited in many chemical analysis applications and in SHM it is no different. A primary X-ray is emitted at a certain, ionizing energy level—usually it is specifically chosen based on the chemical(s) under investigation. The primary X-ray has the effect of ionizing atoms in the target material. Under ionizing radiation, an atom's constituent electron(s) may be knocked out of orbit by the impinging photon (X-ray) or may be excited to a higher energy state. In either case, following removal of this electron by an energetic photon, another electron with a higher energy level drops down to fill its place. The difference in energy between the energy level of the electron "hole" being filled and the energy level that the filling electron left is released as a fluorescent photon (X-ray). There are only a few ways in which this transition can take place depending on which outer shell gives an electron to fill the hole and each scenario results in the emission of a different (secondary) characteristic X-ray. Also, because each element has a unique set of energy levels there are different suites of characteristic X-rays for different elements. In addition, the intensity of these characteristic X-rays is directly proportional to the quantity of atoms in the sample.

Kanada et al. demonstrated this technique as a means of quantifying chloride content in concrete. They selected palladium (Pd) as the X-ray emission source because its Lα X-ray (2.838 keV) is highly effective at exciting chlorine atoms. They determined through trial and error that measurement should be done at low voltages to maximize the peak-background ratio and that X-ray filters (to reduce the background) could be discarded as chlorine is light enough to be excited by such weak X-rays. In their experiment, however, they were in direct contact with the sample and stipulated that this was necessary as X-ray fluorescence is attenuated through the air.

Gamma ray radiography offers a non-contact assessment of a material's thermophysical properties. Gamma rays are attenuated according to a material's density, just as with X-rays, but they are also attenuated by the presence of moisture in the material's pores. The relationship between gamma ray intensity and moisture content for a given material requires knowledge of the gamma ray intensity transmitted by that same material when it is dry. For materials with uniform thickness and porosity, the transmitted intensity of gamma rays is dependent only on the moisture content of the pores (Nizovtsev et al. 2008).

Neutron radiography, like X-ray radiography, is concerned with the variation in attenuation that makes up the object contrast in the resulting image. While in X-ray radiography this attenuation is determined mostly by the target material's density, attenuation in neutron radiography depends on the scattering and capturing potentialities of the constituent elements (Michaloudaki et al. 2005). These differences have consequences for the applications of these techniques. X-ray radiography is favorable for investigating lighter (lower atomic number) elements because in these atoms X-rays interact mostly with the electrons in the atomic shell(s) in ways defined by Compton scattering, the photoelectric effect, and pair production. Neutrons penetrate much deeper than X-rays—interacting with the nucleons of the atom, ignoring electrons completely—and are more favorable for delineating heavier (higher atomic number) elements. There are two important mechanisms (as far as radiography is concerned) of neutron interaction in the atomic nucleus: absorption and scattering. While absorption prevents neutrons from reaching the detector, scattering often leaves a diffuse "sky shine" on the image.

Different elements absorb and scatter neutrons differently with no systematic bias. Consequently, neutron radiography is best used as a complement to X-ray radiography despite the similarities between them (Lehmann et al. 2006). This makes neutron radiography popular in SHM applications such as adhesive inspection and quantification of moisture content. Neutron radiography is used far less frequently than X-ray radiography because there are only a few sites in the world where neutrons can be obtained for such use. Typical sample sizes for neutron radiography range from 1 to 20 cm with spatial resolutions ranging from 10^{-5} to 10^{-3} m per pixel. Practical investigations usually achieve a nominal resolution of 0.1 mm on targets with outer dimensions up to 40 cm. The spatial resolution of neutron radiography is determined both by the detector and the beam width. A well-collimated beam that offers parallel beam geometry is really the only practical option, however, so in practice resolution is truly determined by the detector (Lehmann et al. 2006).

Da Silva et al. (2001) describe the development of a computer-automated means of radiographic pattern recognition, specifically for evaluating welding defects. They describe the following morphologic parameters that are observed in this context: geometric format, length, width, grey level (density) and location in the weld bead. The discriminating factors in classifying welding defect classification are a lack of penetration, undercutting, porosity, and linear and non-linear slag inclusions. By developing a hierarchical, linear classification method that expands upon previous success with non-hierarchical methods by treating those classes easiest to separate first, they were able to achieve 85% success in classification of welding defects.

5.0 Remote Monitoring Techniques

5.1 Electro-Optical Imagery and Photogrammetry

Electro-optical (EO) sensors are those electronic sensors which are sensitive to electromagnetic radiation in the visible spectrum. Charge-coupled devices (CCDs) are the most common electro-optical sensors and this section considers the contribution of even these simple digital camera components to structural health monitoring of bridges. Photogrammetry refers simply to the practice of making measurements from photographs and would currently include measurements made from both film photography and electro-optical (digital) photography. Digital photogrammetry has been demonstrated as a viable technique for generating 3D models of structures and structural elements such as medieval bridges and has also been shown to contribute specifically to damage monitoring of such (Arias et al. 2007). While that study did not utilize stereoscopic photogrammetric techniques, others, such as (Maas and Hampel 2006) did.

Aerial photography has long been studied as a method of SHM as it was the first remote sensing method to be developed for any application. Bridge inspection demands a higher resolution from aerial photography than is normally obtained for most applications. Though most aerial photography missions are flown at 5,000 ft and higher, lower altitudes are necessary to achieve the higher resolution (and consequently smaller area imaged) that is required. This technique is called small-format aerial photography (SFAP). While aerial photography is also usually orthorectified (intentionally distorted to more accurately represent ground coordinates with respect to topography), at such low altitudes (e.g. 1,000 ft), SFAP imagery does not need such post-processing (Rice et al. 2010). This technique is often useful only as a qualitative assessment of cracking, corrosion, deflection, or displacement. While feature recognition and qualitative assessment are viable using FSAP, attempts at more rigorous application of the technique have demonstrated its limitations, such as its coarse resolution (e.g. 1.2 cm) which prevent it from being useful for many SHM applications (Liu et al. 2010).

Digital cameras have been used most successfully for vertical displacement or vibration measurements. The advantage of using CCDs lies in their low cost and high sensitivity to light, although for some applications it can actually be cost-prohibitive or otherwise impossible to achieve the resolution required. One method involves image processing techniques such as pixel identification and edge detection (Chan et al. 2009) that amounts to “blowing out” all background elements to accentuate the structural element of interest. The same study also refers to a “sub-pixel displacement identification measurement” (SPDIM) method that boosts the accuracy of CCDs to that of traditional displacement transducers. Another study has demonstrated the viability and high-accuracy of real-time displacement measurement with image processing techniques

(Lee and Shinozuka 2006). Accuracy of this technique has been quantified to 0.1-1.0 mm for bridges with a fundamental frequency of up to 5 Hz (Olaszek 1999). Another survey using three CCDs measured displacements of a steel beam due to temperature variations of up to 1,200°C with an accuracy of 0.7-1.3 mm (Fraser and Riedel 2000).

Shearography is a full-field video imaging technique that was first developed for strain measurements and now is sufficient enough to do so in real-time over large areas. The technique measures out-of-plane deformation from a fringe pattern generated by two images, one of which is sheared or rotated from the other. The area of concern is illuminated by a laser once before and then after a structure element is loaded. If the element contains a flaw, then strain concentration is induced in that vicinity, and that in turn induces surface strain anomalies. These surface strain anomalies are measured as fringe anomalies and thus the location of the flaw, provided that it is not too deep, can be determined (Chang and Liu 2003). Shearography is related to speckle photography.

Fringe projection interferometry (FPI) is another optical technique is a technique very similar to speckle pattern interferometry (SPI), however, instead of producing an interference pattern from a coherent light source (as in SPI), an interference pattern is projected onto the target surface using an incoherent light source. FPI achieves temporal phase shifting, allowing for the determination of phase shifts in a set of images having introduced a known phase shift. For this technique, a camera is used to record at least as many images as there are interference patterns being projected; the camera-target geometry must be known. The final product of FPI, after phase unwrapping and transformation of the surface map, is an image of the target's surface topography. Typical distances to the target range from 10 to 70 feet and as distance increases there is an associated scaling upwards of pixel size (Krajewski 2006).

Multispectral/hyperspectral imagery, of either satellite or aerial origin, is similar to EO imagery but contains a much broader frequency band, providing images in the infrared and thermal bands in addition to those outside the narrow, visual spectrum. 16-band airborne multispectral imagery has been used in characterizing road surface type with up to 86% accuracy and could be extended to characterizing concrete decks on bridges (Brooks et al. 2007).

5.2 Speckle Photography and Speckle Pattern Interferometry

Speckle is a random, deterministic, interference pattern formed when coherent light is reflected from a surface and is typically regarded as undesirable noise in most fields where it is encountered. Speckle patterns are high-contrast, fine-scale, granular patterns with a random intensity (Anderson and Trahey 2006). Speckle is produced by light reflected from most rough surfaces in the real world. Here, the term "rough" means most any material with microscopic imperfections that are on the scale of optical wavelengths.

This random, microscopic roughness contributes randomly phased, interfering radiation to the total observed field. This effect is strongest when monochromatic light is used to illuminate the surface, as speckle patterns produced by different wavelengths are of different dimensions and tend to average one another out. Although two different surfaces may appear to be identical on the macroscopic scale, their optical roughness is always unique on the microscopic scale to the effect that the two can be distinguished by their speckle patterns. Furthermore, speckle can be used to identify deformations or displacements by comparing speckle patterns of the same surface.

The speckle phenomenon can be observed in most any signal composed of independently-phased, additive components with both amplitude and phase information (e.g. coherent radar, ultrasound). The components of such a signal constitute a “random walk” when they are added together provided they each have random directions in the complex plane. This can result in constructive or deconstructive interference and thus the observed signal may be large or small (Goodman 2004). There are three distinct ways in which speckle patterns change due to surface alterations: a displacement gradient (strain) or local rotation is induced, rigid translation (displacement) of the surface, or a morphological change under which the initial and final states are totally unrelated—this can consist of excessive elastic strain, surface tilt, plastic deformation, or translation or rotation of the target surface.

Applying speckle patterns to structural health monitoring began with *interferometric* techniques such as shearography and electronic speckle pattern interferometry (ESPI). In the latter, real-time fringe patterns are analyzed by comparing a live camera image with a stored reference speckle pattern. These interferometric or *correlation* techniques are contrasted with *speckle photography*, which involves the simple translation of speckle patterns with no use of phase information. The advantage of ESPI is that it has intrinsic resistance to ambient vibration and other sources of environmental noise. The technique utilizes a laser light split into two branches and then expanded in each. One is used to illuminate the target object while the other serves as the stored reference speckle pattern (after it is passed through a diffuser).

After collection, the two speckle patterns collected are made to interfere with one another. Complex calculations are required to deconvolve the output, but computers receiving output from camera CCDs can perform them rapidly. Pedrini and Tiziani (1994) describe a double-pulse ESPI with which three-dimensional deformation can be determined using three directions of illumination and one direction of observation (take two images closely space in time from one camera). Phase-shifting allows for improved signal-to-noise ratio and the real-time calculation of wrapped phase maps. However, these data remain esoteric to most users, including important end-users (e.g. civil engineers, bridge inspectors and managers). Post-processing techniques are necessary for phase unwrapping, ultimately generating “snapshots” of discontinuities or displacement/strain fields. Provided sufficient temporal resolution, temporal phase unwrapping (as opposed to spatial phase unwrapping) is preferred as it allows the extraction of high-quality phase maps and absolute (total since start of process) displacement fields. Coggrave and Huntley (2004) describe an innovative method of implementing these post-processing techniques in real-time by means of a pipeline image processor. Speckle patterns can also be preferentially improved by means of a high-pass filter, removing variations in mean speckle intensity.

In computer speckle interferometry (CSI), speckle patterns are imaged directly by a CCD array and post-processed by consecutive, two-dimensional fast Fourier transforms (FFTs). This derives the off-center peaks, corresponding to degree and direction of in-plane motion (Steckenrider and Wagner 1995). However, this requires certain assumptions about the loading conditions be met. In all speckle photography, the threshold of detection is of the size that individual points on a surface are displaced greater than the speckle size (this holds for speckle photography only and is not desirable for speckle correlation). However, this deformation should not be so great that it induces the local deformation of small regions or the deformation of the entire image. These conditions lead to decorrelation (distortion or loss of visibility of fringes) and the loss of accurate quantitative information about in-plane surface displacement. Steckenrider and Wagner (1995) describe a technique called computed speckle decorrelation (CSD) which combines CSI with intentional decorrelation to allow regions of deformation to be discerned as well as quantitative measurement of correlation. CSD boasts hardware-based image processing that allows for full-frame image analysis and display once every second. Partial-frame analysis can display images at rates approaching that of video frame rates (e.g. 30 frames per second). With the use of a long-distance microscope objective, resolution down to 10 µm can be achieved.

CSI and CSD are both variations of a more general speckle photography technique called digital speckle correlation (DSC) allows for the comparison of two speckle patterns captured at different points in time—say, before and after deformation has occurred—which does not require more than one camera. These two speckle patterns, when combined, are referred to as a *specklegram*. The relative displacement of the correlated patterns can be used to generate Young’s fringes or isothetic fringes which allow for the calculation of displacement and displacement gradient (strain).

Speckle photography and speckle interferometry/correlation have been combined to overcome the limitations imposed by decorrelation. Effects such as mechanical play, rotations, and surface tilt are hard to avoid in engineering applications and they all result in the disappearance of fringes when speckle motion becomes too large. In some areas these effects can be controlled. Variation in laser output energy can be minimized through the use of pulsed lasers and pointing stability; cooled detectors also diminish thermal noise. When these controls are ineffective or irrelevant, other techniques have to be employed. One is to use speckle photography to compensate for speckle motion before performing phase reconstruction in interferometry (Molin et al. 2004).

Other applications of speckle patterns have been investigated but few have been rigorously applied. Elsholz (2005) provides the theoretical groundwork necessary for describing the roughness of a surface based on coherent light scattering. Gulker et al. (2005) describes the use of ESPI in investigating the process of salt crystal growth and the deformation it induces in porous materials. Their experiment, however, was conducted on a very small scale with a microscope objective fitted to the ESPI and a scanning electron microscope (SEM) used for visualization. High-resolution ESPI has been employed in the detection of aircraft corrosion on a scale of 40 mm using both thermal and vacuum loading—the latter also allows for quantitative calculation of deformation fields as the load is well-defined (Jin and Chiang 1998).

In another experiment, the 3D displacement of a plate 4 cm^2 in area was measured using a pair of cameras in stereo and achieved a 4-11% error without coherent light. So-called “white light” speckle interferometry in the frequency domain is popular in engineering applications due to its less stringent demands on measurement illumination and ambient vibration control. These and other interferometric techniques demonstrate the potential for 3D displacement measurements with simple binocular, stereoscopic imaging, eliminating the need for complex light paths used in speckle pattern correlations (Ji et al. 2008).

5.3 Interferometric Synthetic Aperture Radar (IfSAR)

IfSAR (sometimes InSAR) compares pixel-by-pixel differences in phase between two synthetic aperture radar (SAR) images in order to determine changes in surface deformation or ground topography during the time interval that occurred between the two images. Microwave differential interferometry is a very similar technique for mapping displacement phenomena.

Though many sophisticated SAR instrumentation is installed on Earth-orbiting satellites, many of these instruments are not practical for monitoring structures on Earth for despite their sufficient accuracy, they generally lack the resolution or imaging time required for SHM. Consequently, the techniques described here are ground-based (Pieraccini et al. 2004). Generating two SAR images for this purpose requires having two side-looking antennae, separated by a known baseline, ready to receive backscattered signals from a transmitting antenna. This enables the target to be scanned from two different antenna positions. The phase and amplitude of the backscattered signal is stored in each pixel, but it is the phase that reveals the most significant information for terrestrial scanning and SHM applications because it enables the generation of a digital surface model (DSM) or other 3D model (Baran 2009).

For IfSAR experiments in the SHM of bridges, the antenna needs to image multiple sections of the structure from different angles. Generally, displacement in a non-radial direction can be estimated from the displacement along the radar's line of sight (recall that static radar measurements represent movement only in this direction). Pulses are typically transmitted at a 20-50° look angle. As the pulse spreads geometrically from the antenna the reflections of this transmitted energy are recorded as time series. Consequently, different targets positioned at the same distance from the antenna cannot be distinguished (a phenomenon known by *foreshortening* and *layover*). EM *shadows* and multipathing are other limitations of IfSAR (Baran 2009). IfSAR is capable of operating under all weather conditions, however, due to the signal's generally long wavelength, though this can be altered to achieve different degrees of penetration.

Gentile et al. (2008) describe their IBIS-S (image by interferometric survey) sensor that is based on both wideband and interferometric techniques and was developed to measure the deflection of several points on a structure at a sensitivity of better than 0.02 mm—a goal which, if achieved, would make the system the most accurate, stand-off sensor system for the remote monitoring of displacement and deflection in civil engineering structures.

IBIS-S is a coherent radar system, meaning it preserves the phase information of received signals. The central frequency is 16.75 GHz and the antenna can be rotated in any direction. The bandwidth scanning rates are as high as 200 Hz and the sampling interval is 0.005 s. These characteristics make the system suitable for dynamic monitoring and waveform definition of acquired signals (Gentile et al. 2008). IBIS-S is available for commercial purchase and use by Olson Instruments, Inc.

6.0 Exceptional Materials and Structures

6.1 Fiber-Reinforced Polymer Composites

Fiber-reinforced polymer (FRP) composites vary in the composition of constituents but in general the matrix is made up of some polymer and the reinforcement consists of fibers. The most commonly used fiber types are glass (GFRP), carbon, and aramid synthetics (Kevlar); boron, silicon carbide, alumina, and others are used in more specialized applications. These reinforcement fibers are crucial to load transfer. The reinforcement properties are strongest in the direction of the fibers and weakest in directions perpendicular, or transverse, to them. In many applications, structures are not loaded in a single direction, and thus multiple *plies* of FRP composite are layered together randomly to produce a *laminate* consisting of fibers in multiple, random directions.

For the past 50 years, FRP composites have seen limited use in maintenance and construction of civil engineering structures. The corrosion of steel elements in traditional, reinforced concrete has generated interest in FRP as an alternative. Furthermore, FRP offers high strength, stiffness, and durability for low density. In addition to these advantages, FRP composites are easy to install, versatile, and are electromagnetically neutral. FRP composites have been used as pre-stressing tendons dowels in addition to their straightforward use as grid and bar reinforcements.

In maintenance applications, FRP laminates have been applied externally to structures such as reinforced concrete beams in order to increase their load carrying capacity. Li and Liu (2001) note that glass epoxy jackets are commonly used to reinforce concrete bridge collars. In new construction, FRP composites have not found widespread acceptance simply due to the lack of long-term studies of their reliability and structural integrity (Rao 2007). In order to assess their performance, monitoring techniques that are specific to this special material need to be developed, and that is the focus of this section.

Rao (2007) describes several signs of degradation that would be potential targets of structural health monitoring in FRP composites: cracks, matrix micro-cracks, fiber breakage, fiber/matrix debonding, and impact damage which manifests as delamination or large matrix cracks. Rao (2007) goes on to describe how infrared thermography, ultrasonic emissions, acoustic emission, microwave radar, ground-penetrating radar, magnetic, radiography, and optical non-destructive testing techniques have been employed to identify, characterize, and quantify damage to FRP composite structures. In this section, a small number of the studies considered by Rao (2007) have been briefly summarized.

Bates et al. (2000) demonstrated the use of ultrasonic and transient halogen lamp thermography in the inspection of impact damage in FRP composite materials. They found that lock-in thermography was more effective at detecting non-uniform radiation than transient thermography, indicating that lock-in thermography is the preferred choice for curved or other surfaces where geometric effects make uniform heating harder to attain. In FRP composite structures, using infrared thermography, air blisters the size of 16-30 mm have been detected at a distance of up to 20 m (Hu et al. 2002) and delaminations and debonding on the order of 1/16 of an inch thick have been resolved (Halabe et al. 2005). Meola et al. (2004) carried out extensive tests of the geometrical limitations of defect detection in composites and concluded that carbon fibers permit deep investigation due to their higher conductivity and diffusivity and that, intuitively, decreasing size and increasing depth of defects lead to decreased contrast though thickness has a stronger, positive correlation with contrast then size or depth.

Doyum and Durer (2002) describe using the Automated Ultrasonic Scanning System (AUSS), a computer-controlled ultrasonic testing and data collection system, to identify and quantify the size of defects such as planar voids, core damages, and water/hydraulic intrusion in honeycomb composite structures. Hsu et al. (2002) also describe testing composite honeycomb structures—imaging the internal features and evaluating their conditions—using an air-coupled ultrasonic technique with piezoceramic transducers at 50, 120, and 400 kHz. Roth et al. (2003) demonstrated the ability to distinguish delamination, density variation, and microstructural variation in silicon infiltration, and crack space indication in SiC/SiC and C/SiC composites. Hosur et al. (2004) evaluated damage from a high-velocity impact in both stitched and unstitched woven carbon/epoxy composites and concluded that the damaged area is largest in satin weave laminates when compared to plain weave laminates. Imielinska et al. (2004) found that the air-coupled, ultrasonic C-scan technique is capable of detecting impact damage to carbon/epoxy plates as thin as 0.3 mm. Berketis and Hogg (2004), with GFRP composites that had been soaked continuously for two years to induce serious matrix damage, demonstrated how ineffective water-coupled ultrasonic emissions can be when evaluating saturated or water-immersed specimens as the water-damaged areas become invisible to ultrasound; use of an air-coupled ultrasound instead restored the ability to detect water-damaged areas. (Godinez-Azcuaga et al. 2004) used the ultrasonic C-scan technique to reveal debonding, cracks, and delamination in FRP-wrapped concrete columns and bridges.

Santulli (2000) used acoustic emissions to characterize defect areas in impacted glass-woven laminates 5 mm thick and concluded that a coarser weave cases damage to extend over a larger area while there is less damage in mat/polyester laminates of the same material. Amoroso et al. (2003) exhibited the detection and characterization of impact damage in FRP composites utilizing acoustic emission and were able to identify delamination, matrix microfracture, and fiber failure. Stepanova et al. (2004) used stress tests to monitor the fracture process in Organit-10T composite material and found that the onset of fracture could be anticipated from the distribution of acoustic amplitudes.

Zhang and Richardson (2005) demonstrated the sensitivity of optical measurements in detecting barely visible impact deformation; they used both ESPI and an Optical Deformation and Strain Measurement System (ODSMS) to identify the geometry of the damage and for strain classifications. Ambu et al. (2006) showed that holography and ESPI could be used to identify damage in thin FRP laminates with an efficient dependent on the through-thickness location of the delaminations, though the ESPI technique suffered from high noise that reduced the ability to quantify impact damage. Although holography demonstrated higher sensitivity than ESPI in this experiment, it was unable to resolve delaminations lying at interfaces more than 0.7 – 0.8 mm from the impacted surface. Hatta et al. (2005) compared three techniques including ESPI in the damage detection of carbon-carbon composites. With ESPI they were able to clearly observe delamination in carbon-carbon laminates as well as splitting, micro-cracking, and unstable zigzag crack extension.

Li and Liu (2001) used 10 GHz microwave radar and an algorithm for inverting dielectric constants to investigate air-filled voids (debonding) in glass epoxy jackets applied to concrete bridge collars. They achieved a resolution of 0.43 cm using dielectric lenses to focus the radar beams and it is likely that even higher resolution might be achieved at higher frequencies. Though their technique requires operation in extremely close proximity to the target, AbouKhousa and Qaddoumi (2004) have shown how microwave radar can be applied in the near-field to detect subsurface inclusions. Kharkovsky et al. (2006) also demonstrated a dual-polarized, near-field microwave reflectometer applied to carbon fiber-reinforced polymer (CFRP) composites and were able to detect debonding of a region 6 by 8 cm in size in a tilted (severe standoff distance variation) sample. Perhaps the most impressive achievement in this area is by Stephen et al. (2004) who utilized an automated scanning mechanism in conjunction with a near-field microwave reflectometer in the X-band and an open-ended rectangular waveguide to detect delamination between CFRP laminates and concrete substrate.

The efficacy of ground-penetrating radar (GPR) in this arena is highly variable with frequency. At lower frequencies (~1 GHz) the technique fails to resolve shallow defects but at higher frequencies (>2 GHz) the depth of penetration is compromised. Dutta (2006) utilized ground-coupled GPR at 1.5 GHz to detect water-filled voids down to 1.4 inches in diameter (the technique is incapable of detecting air-filled voids). Hing (2006) also used ground-coupled GPR at 1.5 GHz in addition to 2 GHz horn antennae for detection of defects in FRP bridge decks. The study reinforced the knowledge that neither antennae type could detect air-filled voids and that the 1.5 GHz ground-coupled antenna was superior to the 2 GHz horn antennae in detecting water-filled voids.

The field of structural health monitoring with radiographic techniques seems much less prolific than others, but Rao (2007) notes that X-ray radiography has been shown to be effective at detecting water intrusion, density change or deformation of the core, and also air-filled voids. Doyum and Durer (2002) used X-ray radiography to characterize and classify defects unique to honeycomb structures and showed that the technique was much more effective than ultrasound.

Finally, Rao (2007) summarized defect detection done using a Superconducting Quantum Interference Device (SQUID), a very sensitive magnetic (three orders of magnitude more so than conventional magnetometers) flux-to-voltage transducer that utilizes the effect of quantum interference to detect internal flaws in both ferromagnetic and non-ferromagnetic conducting materials. SQUIDs come in two types, or two types of operation: low or high critical temperature (T_C). Hatta, Aly-Hassan (2005) used a low T_C SQUID to detect damage in notched carbon-carbon composites. This technique usually requires contact with the sample for current injection, but Hatsukade et al. (2002) demonstrated a non-contact SQUID technique in which they induced a current in the target using a U-shaped ferrite core and low-frequency current (150 mA at 300 Hz). The peak amplitude of the response they measured compared very well with the direct contact (current injection) method and they concluded the non-contact technique could be applied to very thick carbon fiber composites.

7.0 Case Studies

7.1 Commodore Barry Bridge, Philadelphia, PA

Described by Aktan et al. (2000), this 3288-ft long bridge consists of two anchor spans, two cantilever arms, and a central suspended span. The bridge is instrumented with environmental monitoring systems that report wind speed in three directions and ambient temperatures in several locations once every second. Additional sensors are in place to monitor the bridge's live load in real time. Aktan et al. (2000) also indicated that tilt and displacement sensors were being installed where inadvertent motion was anticipated; these would determine both the movement history and the displacement kinematics in three dimensions.

These and other data from controlled load tests and ambient vibration tests have been collected since the sensors were first installed in 1998. The data have been interpreted in terms of the bridge's mechanical characteristics and its loading and response environment with a 3D finite-element model. The controlled test data are used to calibrate and validate the analytical model (Aktan et al. 2000).

Plans exist to outfit the bridge with a new array of modern, remote sensors that will be part of a high-speed fiber-optic local-area network (LAN), communicating with two data acquisition systems at the towers which will communicate wirelessly with a bridge data server. This server will host real-time data streams and allow for the remote monitoring and manipulation of data acquisition, viewing of data and bridge imagery, as well as archival. Weigh-in-motion (WIM) and weather monitoring systems distant from the bridge itself will also communicate wirelessly with the bridge data server. Other planned sensor modalities include accelerometers, resistance strain gauges, vibrating wire strain gauges, thermistors (temperature-sensitive resistors), long-gauge fiber optic displacement wires, and vibrating wire crackmeters and tiltmeters.

Most interesting is the capability of corresponding video images of truck positions with WIM systems and the strains they report at those positions. Eventually, millimeter-level GPS and acoustic weld sensors will be incorporated to monitor the global geometry and welding fatigue, respectively.

These multiple data sources must be integrated in a meaningful way, and currently the Commodore Barry Bridge SHM relies on the LabView software program, graphical programming environment that allows for sophisticated data acquisition, instrument control, and signal processing. Deck and driving conditions and traffic levels as well as bridge element temperatures and strains are all monitored in real time using LabView. The goal of the user interface is to allow bridge managers to react to incidents and anomalies immediately by alerting them once certain conditions are detected. Images of the user interface are provided in Atkan et al. (2000) as well as a detailed description of the phenomenological laboratory model being developed by Drexel University researchers.

7.2 Golden Gate Bridge, San Francisco, CA

(Kim et al. 2007) describe a wireless sensor network installed on the south tower and 4200-ft long main span of the iconic Golden Gate Bridge. Their installed sensor network consisted of 64 accelerometer sensors measuring ambient vibration accurately to 30 µG. The chosen sampling rate was 1 kHz with a time aperture of less than 10 µs and data were streamed at 441 B/s with pipelining.

One of the project requirements was the ability to detect signals with peak amplitudes as low as 500 µG. This was a serious constraint on the noise floor of the entire system, installation error, and temperature variation. To this end, each of the microelectronic mechanical systems (MEMS) that comprise an accelerometer node has a thermometer to measure acceleration temperature. The high sampling rate employed was also necessary in order to describe the local modes of vibration. The sensor software was based on TinyOS—an operating system specifically designed for MEMS.

7.3 Tsing Ma Bridge, Hong Kong, China

With a main span length of 1,377 m The Tsing Ma bridge has the distinction of being the longest suspension bridge to carry both highway and railway traffic (Chan et al. 2006). Highway traffic uses dual three-lane roads on top of a covered deck for two railway lines and two emergency roadways for use in periods of very high wind. Since the bridge was commissioned on May 22, 1997, the bridge has been monitored by the Wind and Structural Health Monitoring System (WASHMS), which is also used to monitor the conditions of two other cable-supported bridges in Hong Kong: the Ting Kau Bridge and the Kap Shui Mun Bridge.

WASHMS is comprised of a permanent sensor network of 774 nodes, making it—along with the Ting Kau and Kap Shui Mun bridges—one of the most heavily instrumented bridges in industry (Ko et al. 2000). These sensors include accelerometers, strain gauges (110 installed on the bridge deck), displacement transducers, level sensors, GPS sensors anemometers, temperature sensors, and weigh-in-motion (WIM) sensors all connected to a data acquisition and processing system. WASHMS has been used to test the efficacy of a new monitoring system using fiber Bragg grating (FBG) sensors developed by Hong Kong Polytechnic University. These FBG sensors are multiplexed and capable of simultaneous strain and temperature measurement as well as temperature-independent strain measurements. Their SHM system using FBG sensors is called DEMINSYS (demultiplexing/interrogation system) and boasts a resolution and accuracy of 1 pm and 10 pm, respectively, using a wavelength detection array comprised of sensitive charge-coupled device (CCD) sensors. The system uses a broadband light source operating around 1550 nm and can achieve a sampling rate of up to 20 kHz. Chan et al. (2006) found that DEMINSYS can clearly and correctly detect dynamic strain responses to the passage of trains on the bridge(s).

7.4 Vernon Avenue Bridge, Barre, Massachusetts

This bridge is a 150 foot three-span continuous bridge that was built in the summer of 2009. The eight inch cast-in-place deck is supported by six steel girders. The sensors were placed on the structure during the construction process to capture the full strain history of the bridge. Vernon Avenue Bridge has a total of 100 strain gauges, 36 girder thermistors, 30 concrete thermistors, four bi-axial abutment tiltmeters and 16 biaxial accelerometers. These were placed at 13 different stations across the span of the bridge in which the data is collected using iSite® data acquisition boxes provided by Geocomp, INC. (Bell et al. 2010). This data was collected at different milestones during construction and has been collected ever 5 minutes since the concrete deck was poured.

Two different models are being created to model the bridge. The models are to model the actual response of the structure with the safety factors removed. The modeling of the bearing pads is difficult with defining the boundary conditions on the bridge, and all the different components of the bridge needed to be taken into account with the models to achieve the desired accuracy. One of the models is being drawn in great detail as a finite element model that makes use of solid elements to represent the concrete deck and shell elements to model the steel girders. This model was drawn in SAP2000® to be extruded along the length of the bridge. All assumptions are to be taken out of this model to try and provide the most accurate baseline available. Temperature gradients are also to be included in the model to allow the calibration with temperature. This model is to be created with all the components to provide the most realistic model possible (Bell et al. 2010).

The other model is being created using BrIM in SAP2000® to form the initial geometry for the bridge. The BrIM will then be turned off to change the model from designed based to monitoring based. This element is to be created with frame elements instead solid and shell elements of the previous model. With this model beam elements represent the girders and support piers, shells and/or brick elements represent the deck, and spring elements to represent boundary conditions. These two models than can be compared on how well they predict the behavior of the bridge compared to the amount of time used to create the model (Bell et al. 2010).

7.5 Cut River Bridge, Michigan

The Cut River Bridge was outfitted with different sensors in 2007 by Michigan Department of Transportation (MDOT). The Cut River Bridge is a steel truss bridge that is supported by two piers with a 125 foot anchor arm and a125 foot cantilever arm each for a total span of 500 feet. This was completed to go along with the Mackinac Bridge sensing system, so the data from the Cut River Bridge is sent wirelessly to the computers there in which MDOT has access to the data. The whole system is run from five solar panels which charge batteries until up to sixteen days of charge is available.

There are eight wireless fiber optic strain gages on each side of the bridge along with two temperature sensors for a total of sixteen fiber optic strain gages and four temperature sensors. The location of the strain gages can be seen in Figure 1 where the arrows are pointing to. There are two bridge deck environmental sensors placed on the bridge. The temperature and environmental sensors can be used to correlate their values to the strain gages to see how the strains are affected by temperature and other environmental factors. The bridge is also equipped with one wireless weigh-in-motion sensor along with two traffic monitoring sensors. This allows for the correlation of loads crossing the bridge with the strains on the bridge. Two close circuit television cameras are also in place on a seventy foot tower which can be used to confirm the values of the weigh-in-motion sensor and the traffic monitoring sensors.

Figure 1: Location of Sensors on Cut River Bridge

The data is to be used to develop correlations and comparisons between the actual bridge service loads and those used to design the bridge. MDOT is looking to establish a baseline from the data that they are collecting now to use in the future. They are hoping to be able to examine future trends or changes in behavior and maintain the safety of the bridge along with being able to use the data to help with future maintenance planning for the bridge.

7.6 Field Monitoring of Four Integral Abutment Bridges, Pennsylvania

This study was the monitoring of four integral abutment bridges (IABs) for the use of gaining an understanding of different forces on these bridges. This studied looked at the time dependent and thermal effects on the bridge members. Due to environment concerns the four bridges weren't open for traffic for between 2 to 5 years from when the monitoring started. This allowed the study to look at just the effects of time and thermal changes to the bridges. The goal of the project was to determine how these effects could be better understood when designing IABs (Kim and Laman 2009).

Table 4: Field Monitored IAB Description

Bridge No.	Girder Type	Integral Abutment	Abutment Height (ft-in)	Span Lengths Total Length (ft)	Number of Instruments
109	PennDOT 28/78*	Both	11-6	88-122-122-88 = 420	64
203	AASHTO V	North Only South Fixed	19-0	47-88-37 = 172	64
211	PennDOT 28/78*	Both	14-1	114	64
222	PennDOT 24/48*	Both	13-1	62	48

* PennDOT DM-4 (2007)
†Note: 1 inch = 0.0254 m, 1 ft = 0.3048 m.

There were a total of 240 sensors placed on the four bridges which were constructed from precast prestressed concrete girders with cast-in-place deck. The different properties of the bridge can be seen in the table below. There were multiple vibrating wire-based instruments placed on the bridge include: backfill pressure cells, abutment displacement extensometers, girder axial force and moment strain gages, girder tiltmeters, abutment tiltmeters, pile moment and axial force strain gages, and approach slab sister-bar strain gages.

The results of the extensometers for measuring displacement on the abutments showed that the top and bottom sensors had a wide range of movement for the given bridges. The maximum displacement ranges for the top were from 0.056 in to 1.935, and the bottom was from 0.186 in to 2.029 in over the period of when the bridge was completed as early as 2003 to 2009. The results of displacement are in a sinusoidal shape with the peak during the summer and the valley during the winter. Both abutment and girder ration were measured using a tiltmeter. The results for the abutment rotation varied from 0.139 to 0.322 degrees for the interior location and 0.096 to 0.187 degrees for the exterior location. The results for the girder rotation varied from 0.157 to 0.225 degrees for the interior location and 0.135 to 0.255 degrees for the exterior location.

Other results found were pile moment and axial force, girder moment and axial force, approach slab strain, ambient temperature and structural temperature. With all these results the several conclusions could be reached. The temperature had the biggest affect on the different properties measured in this study. There was no significant change in the properties once traffic started showing that this wasn’t a significant load on the bridge.

7.7 Bridge Monitoring TestBed

This case study consisted of four span 90 m long bridge that was out fitted with TestBed monitoring system along with a decision support system. The TestBed was developed at the University of California, San Diego. There are a total of 20 accelerometers placed in one of the box girders along the length of the bridge. These are wired to a data collection system that sends the information to a computer. There was also a camera set up to collect images of the traffic traveling over the bridge to allow the correlation of the accelerations values with the type of load crossing the bridge (Fraser et al 2010).

Using a decision support system they are able to correlate the load passing over the different sensor as well as the reading from the sensors to see how the load affected the structure. A website was developed to retrieve and disseminate the data for any time period desired. The web page can be seen in Figure 2. This system allows for the view of data from anytime period desired. They are developing a vehicle detection system in which the system can identify different vehicle sizes depending on how many pixels the vehicle takes up at know locations. This allows for the user to not have to identify the size of the vehicle since the system would do this.

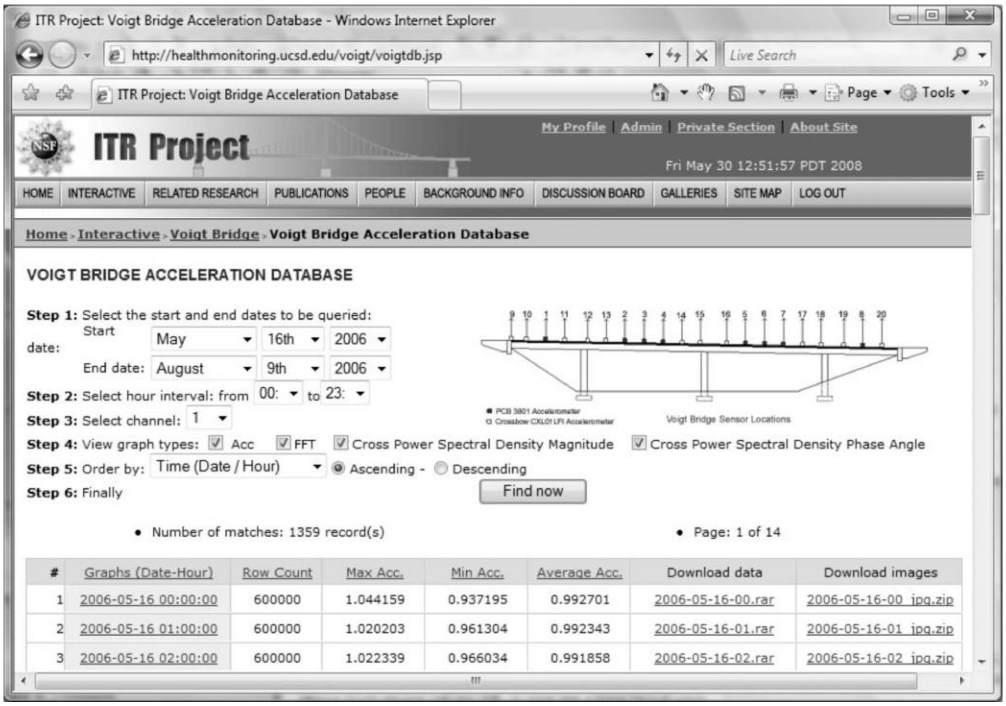

VOIGT BRIDGE ACCELERATION DATABASE

Step 1: Select the start and end dates to be queried:
Start date: May 16th 2006
End date: August 9th 2006
Step 2: Select hour interval: from 00: to 23:
Step 3: Select channel: 1
Step 4: View graph types: ☑ Acc ☑ FFT ☑ Cross Power Spectral Density Magnitude ☑ Cross Power Spectral Density Phase Angle
Step 5: Order by: Time (Date / Hour) ● Ascending - ○ Descending
Step 6: Finally

- Number of matches: 1359 record(s)
- Page: 1 of 14

#	Graphs (Date-Hour)	Row Count	Max Acc.	Min Acc.	Average Acc.	Download data	Download images
1	2006-05-16 00:00:00	600000	1.044159	0.937195	0.992701	2006-05-16-00.rar	2006-05-16-00_jpg.zip
2	2006-05-16 01:00:00	600000	1.020203	0.961304	0.992343	2006-05-16-01.rar	2006-05-16-01_jpg.zip
3	2006-05-16 02:00:00	600000	1.022339	0.966034	0.991858	2006-05-16-02.rar	2006-05-16-02_jpg.zip

Figure 2: Web page for quering, browsing and downloading the recorded accelation and video data

8.0 References

AbouKhousa, M. and N. Qaddoumi (2004). Near-field microwave imaging of subsurface inclusions in laminated composite structures. 16th World Conference on Nondestructive Testing. Montreal, Canada.

Aktan, A. E., F. N. Catbas, M. Pervizpour, E. Kulcu, K. Grimmelsman, R. Barrish, X. Qin. (2000). Real-time bridge health-monitoring for management. Second Workshop on Advanced Technologies in Urban Earthquake Disaster Mitigation. Kyoto University, Drexel Intelligent Infrastructure Institute.

Alqennah, H. (2000). Detection of subsurface anomalies in composite bridge decks using infrared thermography. Department of Civil and Environmental Engineering. Morgantown, WV, West Virginia University. Master of Science in Civil Engineering: 95.

Ambu, R., F. Aymerich, F. Ginesu, P. Priolo. (2006). "Assessment of NDT interferometric techniques for impact damage detection in composite laminates." Composites Science and Technology 66(2): 199-205.

Amey, A. (2009). "Beyond State-Level Bridge Counts – Alternative Performance Measures for Evaluating Bridge Conditions." 2010 TRB Annual Meeting.

Amoroso, M. P., C. Caneva, F. Nanni, M. Valente. (2003). Acoustic emission performance for damage monitoring of impacted FRP composite laminates. Review of Progress in Quantitative Nondestructive Evaluation:Volume 22, Bellingham, Washington (USA), AIP.

Anderson, M. E. and G. E. Trahey. (2006, February 15, 2006). "A beginner's guide to speckle." A seminar on k-space applied to medical ultrasound Retrieved February 22, 2010, 2010, from http://dukemil.bme.duke.edu/Ultrasound/k-space/node5.html.

Angelidis, N., C. Y. Wei, P. E. Irving. (2004). "The electrical resistance response of continuous carbon fibre composite laminates to mechanical strain." Composites Part A: Applied Science and Manufacturing 35(10): 1135-1147.

Ansari, F. (2005). "Fiber optic health monitoring of civil structures using long gage and acoustic sensors." Smart Materials and Structures 14(3): S1-S7.

Arias, P., J. Armesto, D. Di-Capua, R. González-Drigo, H. Lorenzo, V. Pérez-Gracia. (2007). "Digital photogrammetry, GPR and computational analysis of structural damages in a mediaeval bridge." Engineering Failure Analysis 14(8): 1444-1457.

Arunachalam, K., V. R. Melapudi, L. Udpa, S. S. Udpa. (2006). "Microwave NDT of cement-based materials using far-field reflection coefficients." NDT & E International 39(7): 585-593.

ASCE, A. S. o. C. E. (2009). "Bridges | report card for America's infrastructure." Retrieved February 22, 2010, 2010, from http://www.infrastructurereportcard.org/fact-sheet/bridges.

Baran, I. (2009). Airborne InSAR and LiDAR compared.

Bates, D., D. Lu, G. F. Smith, J. Hewitt, (2000). Rapid NDT of composite aircraft components using lock-in ultrasonic and halogen lamp thermography. Nondestructive Evaluation of Aging Materials and Composites IV, Newport Beach, CA, USA, SPIE.

Bell, E., J. Sipple, P. Lefebvre, J. Phelps, B. Brenner, M. Sanayei. (2010). "Instrumentation, Modeling and Monitoring of a Concrete Bridge from Construction through Service." Transportation Research Board 2010 Annual Meeting.

Berketis, K. and P. J. Hogg (2004). "Effectiveness of non-contact ultrasonics for damage detection on wet GFRP composites."

Beyea, S. D., B. J. Balcom, T. W. Bremner, P. J. Prado, D. P. Green, R. L. Armstrong, P. E. Grattan-Bellew. (1998). "Magnetic resonance imaging and moisture content profiles of drying concrete." Cement and Concrete Research 28(3): 453-463.

Bhalla, S. and C. K. Soh (2004). "Structural health monitoring by piezo-impedance transducers I: modeling." Journal of Aerospace Engineering 17(4): 154-165.

Brooks, C., D. Schaub, B. Thelen, R. Shuchman, R. Powell, E. Keefauver, (2007). TARUT pilot studies technical details report. Deliverable 5.3-B. M. D. o. Transportation, Michigan Tech Research Institute.

Bungey, J. H. (2004). "Sub-surface radar testing of concrete: a review." Construction and Building Materials 18(1): 1-8.

Burleigh, D. D. and R. Bohner (1999). Thermal nondestructive testing (TNDT) of adhesively bonded composite reinforcements applied to concrete civil structures. Nondestructive Evaluation of Bridges and Highways III, Newport Beach, CA, USA, SPIE.

Casas, J. R. and P. J. S. Cruz (2003). "Fiber optic sensors for bridge monitoring." Journal of Bridge Engineering 8(6): 362-373.

Castro, T. A., D. V. Jáuregui, S. R. Maberry. (2009). "A Collaborative Approach for Load Rating of State Owned Bridges." TRB 2010 Annual Meeting.

Chan, T. H. T., D. B. Ashebo, H. Y. Tam, Y. Yu, T. F. Chan, P. C. Lee, E. Perez Gracia, (2009). "Vertical displacement measurements for bridges using optical fiber sensors and CCD cameras -- a preliminary study." Structural Health Monitoring **8**(3): 243-249 10.1177/1475921708102108: 10.1177/1475921708102108.

Chan, T. H. T., L. Yu, H. Y. Tam, Y. Q. Ni, S. Y. Liu, W. H. Chung, L. K. Cheng. (2006). "Fiber Bragg grating sensors for structural health monitoring of Tsing Ma bridge: Background and experimental observation." Engineering Structures 28(5): 648-659.

Chang, P. C., A. Flatau, S. C. Liu. (2003). "Review paper: health monitoring of civil infrastructure." Structural Health Monitoring 2(3): 257-267 10.1177/1475921703036169: 10.1177/1475921703036169.

Chang, P. C. and S. C. Liu (2003). "Recent research in nondestructive evaluation of civil infrastructures." Journal of Materials in Civil Engineering 15(3): 298-304.

Chong, K. P., N. J. Carino, G. Washer. (2003). "Health monitoring of civil infrastructures." Smart Materials and Structures 12(3): 483.

Chung, D. D. L. (2001). "Structural health monitoring by electrical resistance measurement." Smart Materials and Structures 10.

Cochran, A., G. B. Donaldson, L. N. C. Morgan, R. M. Bowman, K. J. Kirk. (1993). SQUIDS for NDT: the technology and its capabilities. Southend-on-Sea, ROYAUME-UNI, Non-Destructive Testing Society of Great Britain.

Coggrave, C. R. and J. M. Huntley (2004). "Real-time visualization of deformation fields using speckle interferometry and temporal phase unwrapping." Optics and Lasers in Engineering 41: 601-620.

Crider, J. S. (2007). Damage detection using Lamb waves for structural health monitoring. Wright-Patterson Air Force Base, Ohio, Air Force Institute of Technology.

da Silva, R. R., M. H. S. Siqueira, L. P. Caloba, J. M. A. Rebello. (2001). "Radiographics pattern recognition of welding defects using linear classifiers." Insight 43(10).

David, L. M., M. D. Todd, G. Park, C. R. Farrar. (2007). "Development of an impedance-based wireless sensor node for structural health monitoring." Smart Materials and Structures 16(6): 2137.

DelGrande, N. and P. F. Durbin (1999). Delamination detection in reinforced concrete using thermal inertia. Nondestructive Evaluation of Bridges and Highways III, Newport Beach, CA, USA, SPIE.

Doyum, A. B. and M. Durer. (2002). "Defect characterization of composite honeycomb panels by non-destructive inspection methods." from http://www.ndt.net/article/dgzfp02/papers/p36/p36.htm.

Dutta, S. S. (2006). Nondestructive evaluation of FRP wrapped concrete cylinders using infrared thermography and ground penetrating radar. Department of Civil and Environmental Engineering. Morgantown, West Virginia, West Virginia University. Master of Science in Civil Engineering: 128.

Elsholz, F. (2005). Rough surface characterization and determination of the RMS roughness from coherent light scattering.

Federal Highway Administration. (1995). "Recording and Coding Guide for the Structure Inventory and Appraisal of the Nation's Bridges." (FHWA-PD-96-001).

Federal Highway Administration. Deficient Bridges By Material Type of Structure by State, accessed at http://www.fhwa.dot.gov/BRIDGE/material.htm. July 7, 2010.

Fraser, C. S. and B. Riedel (2000). "Monitoring the thermal deformation of steel beams via vision metrology." ISPRS Journal of Photogrammetry and Remote Sensing **55**(4): 268-276.

Fraser, M., A. Elgamal, X. He, J. P. Conte. (2010). "Sensor Network for Structural Health Monitoring of a Highway Bridge." JOURNAL OF COMPUTING IN CIVIL ENGINEERING (January/Febuary).

Gentile, C., G. Bernardini, P. Ricci. (2008). "A new interferometric radar for full-scale testing of bridges: ambient vibration tests and operational modal analysis."

Godinez-Azcuaga, V. F., R. D. Gostautas, R. D. Finlayson, M. Miller. (2004). Nondestructive evaluation of FRP wrapped concrete columns and bridges. Structural Materials VI - An NDT Conference, Buffalo, NY, U.S.A.

Goodman, J. W. (2004). Speckle phenomena in optics: theory and applications.

Gueguen, P., V. Jolivet, C. Michel, A. Schveitzer. (2009). "Comparison of velocimeter and coherent LiDAR measurements for building frequency assessment." Bulletin of Earthquake Engineering.

Gulker, G., A. El Jarad, K. D. Hinsch, H. Juling, K. Linnow, M. Steiger, St. Bruggerhoff, D. Kirchner. (2005). Monitoring of deformations induced by crystal growth of salts in porous systems using microscopic speckle pattern interferometry. Lasers in the Conservation of Artwork, LACONA VI Proceedings. Vienna, Austria.

Haeni, F. P., G. Placzek, R. E. Trent. (1992). Use of ground penetrating radar to investigate refill scour holes at bridge foundations. Fourth International Conference on Ground Penetrating Radar, Rovaniemi, Finland.

Halabe, U. B., A. Vasudevan, H. V. S. GangaRao, P. Klinkhachorn, G. Lonkar. (2005). Subsurface defect detection in FRP composites using infrared thermography. Review of Progressive in Quantitative Nondestructive Evaluation, Golden, Colorado (USA), AIP.

Hatsukade, Y., N. Kasai, H. Takashima, A. Ishiyama. (2002). "Non-contact SQUID-NDT method using a ferrite core for carbon-fibre composites." Superconductor Science and Technology 15(12): 1728.

Hatta, H., M. S. Aly-Hassan, Y. Hatsukade, S. Wakayama, H. Suemasu, N. Kasai, (2005). "Damage detection of C/C composites using ESPI and SQUID techniques." Composites Science and Technology 65(7-8): 1098-1106.

Hide, C., S. Blake, X. Meng, G. W. Roberts, T. Moore, D. Park. "An investigation in the use of GPS and INS sensors for structural health monitoring."

Hing, C. L. (2006). Nondestructive evaluation of fiber reinforced polymer bridge decks using ground penetrating radar and infrared thermography. Department of Civil and Environmental Engineering. Morgantown, West Virginia, West Virginia University. Doctor of Philosophy in Civil Engineering.

Hosur, M. V., U. K. Vaidya, C. Ulven, S. Jeelani. (2004). "Performance of stitched/unstitched woven carbon/epoxy composites under high velocity impact loading." Composite Structures 64(3-4): 455-466.

Howard, G. B., C. P. Sturos, T. M. Ahlborn. (2010). "Detection of bridge deck de-laminations using thermal imaging." Roads and Bridges 98(2).

Hsu, D. K., D. J. Barnard, J. J. Peters, V. Dayal, V. Kommareddy.(2002). Nondestructive inspection of composites and their repairs. 6th Join AAA/DOD Aging Aircraft Conference, San Francisco, CA, U.S.A.

Hu, C. W., J. K. C. Shih, R. Delpak, D. B. Tann.(2002). Detection of air blisters and crack propagation in FRP-strengthened concrete elements using infrared thermography. Inframation - The Thermographer's Conference.

Huynh, S. H. and G. Cheng (2000). Low profile ceramic choke. United States, Antom Corporation. 6,040,805.

Imielinska, K., M. Casaings, R. Wojtyra, J. Haras, E. Le Clezio, B. Hosten.(2004). "Air coupled ultrasonic C scan technique in impact response testing of carbon fiber and hybrid composites." Journal of Materials Processing Technology 157(58): 513-522.

Inaudi, D. and B. Glisic (2004). "Combining static and dynamic deformation monitoring with long-gauge fiber optic sensors."

Jenks, W. G., S. S. H. Sadeghi, J. P. Wikswo.(1997). "SQUIDs for nondestructive evaluation." Journal of Physics D: Applied Physics 30(3): 293.

Jerry, J. S. and H. L. C. Roger (2000). Bridge Decks Inspection Using Chain Drag and Ground Penetrating Radar, ASCE.

Ji, X., X. Yang, C. Jinlong. (2008). "3D displacement measurement by white light digital image analysis in frequency domination area."

Jin, F. and F. P. Chiang (1998). "ESPI and digital speckle correlation applied to inspection of crevice corrosion on aging aircraft." Res Nondestr Eval 10: 63-73.

Justnes, H., I. Meland, J. O. Bjoergum, J. Krane, T. Skjetne.(1990). "Nuclear magnetic resonance (NMR)--a powerful tool in cement and concrete research." Advances in Cement Research **3**(11): 105-110.

Kanada, H., Y. Ishikawa, T. Uomoto."Measurement of chloride content in concrete using near-infrared spectroscopy and x-ray fluorescence analysis."

Kang, I., M. J. Schulz, J. H. Kim, V. Shanov, D. Shi.(2006). "A carbon nanotube strain sensor for structural health monitoring." Smart Materials and Structures 15(3): 737.

Kharkovsky, S., A. C. Ryley, V. Stephen, R. Zoughi.(2006). Dual-polarized microwave near-field reflectometer for non-invasive inspection of carbon fiber reinforced polymer (CFRP) strengthened structures. IMTC 2006 - Instrumentation and Measurement Technology Conference. Sorrento, Italy.

Kijewski-Correa, T. (2005). "GPS: a new tool for structural displacement measurements." APT Bulletin 36(1): 13-18.

Kim, W. and J. A. Laman (Nov. 15, 2009). "Long-term Field Monitoring of Four Integral Abutment Bridges." Transporation Research Board 2010 Annual Meeting.

Kim, S., S. Pakzad, D. Culler, J. Demmel, G. Fenves, S. D. Glaser, M. Turon. (2007). Health monitoring of civil infrastructures using wireless sensor networks. Proceedings of the 6th international conference on Information processing in sensor networks. Cambridge, Massachusetts, USA, ACM.

Knecht, A. and L. Manetti (2001). "Using GPS in structural health monitoring."

Ko, J. M. and Y. Q. Ni (2005). "Technology developments in structural health monitoring of large-scale bridges." Engineering Structures **27**(12): 1715-1725.

Ko, J. M., Y. Q. Ni, J. Y. Wang, Z. G. Sun, X. T. Zhou.(2000). "Studies of vibration-based damage detection of three cable-supported bridges in Hong Kong."

Krajewski, J. E. (2006). Bridge inspection and interferometry. Worcester, Massachusetts, Worcester Polytechnic Institute. Master of Science in Civil Engineering: 120.

Krammer, P., M. Willsch, N. Theune, M. Rothhardt.(2000). Novel fiber optic Bragg grating acceleration sensor detection scheme. Proceedings of SPIE, the International Society for Optical Engineering.

Krause, H. J., W. Wolf, W. Glaas, E. Zimmermann, M. I. Faley, G. Sawade, R. Mattheus, G. Neudert, U. Gampe, J. Krieger. (2002). "SQUID array for magnetic inspection of prestressed concrete bridges." Physica C: Superconductivity 368(1-4): 91-95.

Kuang, K. S. C., Akmaluddin, W. J. Cantwell, C. Thomas.(2003). "Crack detection and vertical deflection monitoring in concrete beams using plastic optical fibre sensors." Measurement Science and Technology 14(2): 205-216.

Lau, K.-t. (2003). "Fibre-optic sensors and smart composites for concrete applications." Magazine of Concrete Research 55(1): 16.

Lee, H. M., H. S. Park, I. Lee, H. Adeli.(2005). Displacement measuring model of continuous steel beams using terrestrial LiDAR. 4th World Conference on Structural Control and Monitoring.

Lee, J. and M. Shinozuka (2006). "Real-time displacement measurement of a flexible bridge using digital image processing techniques." Experimental Mechanics 46(1): 105-114.

Lehmann, E., P. Vontobel, R. Hassanein. (2006). Neutron tomography as tool for applied research and technical inspection. Advances in Solid State Physics**:** 389-405.

Li, G. (2004). The effect of moisture content on the tensile strength properties of concrete. Gainesville, Florida, U.S.A., University of Florida. Master of Engineering.

Li, J. and C. Liu (2001). "Noncontact detection of air voids under glass epoxy jackets using a microwave system." Subsurface Sensing Technologies and Applications 2(4): 411-423.

Ling, H.-y., K.-t. Lau, L. Cheng, W. Jin.(2005). "Fibre optic sensors for delamination identification in composite beams using a genetic algorithm." Smart Materials and Structures 14(1): 287-295.

Liu, W., S.-E. Chen, K. Dai, C. Rice, B. Phibrick, E. Hauser, Z. Hu, C. K. Huyck, C. Boyle.(2010). Bridge evaluation through advanced noncontact sensing techniques. Transportation Research Board 89th Annual Meeting. Washington, D.C., Transportation Research Board of IHF National Academies.

Lo, Y.-L. and F.-Y. Xiao (1998). "Measurement of corrosion and temperature using a single-pitch Bragg grating fiber sensor." Journal of Intelligent Material Systems and Structures 9(10): 800-807 10.1177/1045389x9800901003: 10.1177/1045389x9800901003.

Lopes, V., Jr., G. Park, H. H. Cudney, D. J. Inman.(2000). "Impedance-based structural health monitoring with artificial neural networks." Journal of Intelligent Material Systems and Structures 11(3): 206-214 10.1106/h0ev-7pwm-qyhw-e7vf: 10.1106/h0ev-7pwm-qyhw-e7vf.

Lynch, J. P. (2005). "Design of a wireless active sensing unit for localized structural health monitoring." Structural Control and Health Monitoring 12: 405-423.

Lynch, J. P. and K. J. Loh (2006). "A summary review of wireless sensors and sensor networks for structural health monitoring." The Shock and Vibration Digest 38(2): 91-128.

Lynch, J. P., Y. Wang, K. C. Lu, T. C. Hou, C. H. Loh.(2006). "Post-seismic damage assessment of steel structures instrumented with self-interrogating wireless sensors."

Maas, H.-G. and U. Hampel (2006). "Photogrammetric techniques in civil engineering material testing and structure monitoring." Photogrammetric Engineering & Remote Sensing **72**(1): 7.

Maser, K. R. and M. Bernhardt (2000). Statewide bridge deck survey using ground penetrating radar. Structural Materials Technology IV: An NDT Conference. S. Alampalli. Lancaster, PA, Technomic Publishing Company**:** 31-37.

Maser, K. R. and W. M. K. Roddis (1990). "Principles of thermography and radar for bridge deck assessment." Journal of Transportation Engineering 116(5): 583-601.

Masri, S. F., L. H. Sheng, J. P. Caffrey, R. L. Nigbor, M. Wahbeh, A. M. Abdel-Ghaffar.(2004). "Application of a Web-enabled real-time structural health monitoring system for civil infrastructure systems." Smart Materials and Structures 13(6): 1269-1283.

MBE 2008, Manual for Bridge Evaluation, American association of State Highway and Transportation Officials, Washington DC, U.S.A.

Mehrabi, A. B. (2006). "In-service evaluation of cable-stayed bridges, overview of available methods, and findings." Journal of Bridge Engineering 11(6): 716-724.

Meng, X., A. H. Dodson, G. W. Roberts.(2007). "Detecting bridge dynamics with GPS and triaxial accelerometers." Engineering Structures 29(11): 3178-3184.

Meola, C., G. M. Carlomagno, L. Giorleo.(2004). "Geometrical limitations to detection of defects in composites by means of infrared thermography." Journal of Nondestructive Evaluation 23(4): 125-132.

Merzbacher, C. I., A. D. Kersey, E. J. Friebele.(1996). "Fiber optic sensors in concrete structures: a review." Smart Materials and Structures 5(2): 196-208.

Meyendorf, N. G. H., H. Rösner, V. Kramb, S. Sathish.(2002). "Thermo-acoustic fatigue characterization." Ultrasonics 40(1-8): 427-434 10.1016/S0041-624X(02)00155-5: 10.1016/S0041-624X(02)00155-5.

Michaloudaki, M., E. Lehmann, D. Kosteas.(2005). "Neutron imaging as a tool for the non-destructive evaluation of adhesive joints in aluminium." International Journal of Adhesion and Adhesives 25(3): 257-267.

Molin, N. E., M. Sjodahl, P. Gren, A. Svanbro.(2004). "Speckle photography combined with speckle interferometry." Optics and Lasers in Engineering 41: 673-686.

Morey, R. M. (1998). Ground penetrating radar for evaluating subsurface conditions for transportation facilities.

Nizovtsev, M. I., S. V. Stankus, A. N. Sterlyagov, V. I. Terekhov, R. A. Khairulin.(2008). "Determination of moisture diffusivity in porous materials using gamma-method." International Journal of Heat and Mass Transfer 51(17-18): 4161-4167.

Olaszek, P. (1999). "Investigation of the dynamic characteristic of bridge structures using a computer vision method." Measurement 25(3): 227-236.

Olhoeft, G. R. and S. S. Smith (2000). "Automatic processing and modeling of GPR data for pavement thickness and properties."

Panova, A. A., P. Pantano, D. R. Walt.(1997). "In situ fluorescence imaging of localized corrosion with a pH-sensitive imaging fiber." Analytical Chemistry 69(8): 1635-1641 10.1021/ac961025c: 10.1021/ac961025c.

Park, G., H. H. Cudney, D. J. Inman. (2000). "Impedance-based health monitoring of civil structural components." Journal of Infrastructure Systems 6(4).

Park, H. S., H. M. Lee, H. Adeli. (2007). "A new approach for health monitoring of structures: terrestrial laser scanning." Computer-Aided Civil and Infrastructure Engineering 22.

Pedrini, G. and H. J. Tiziani (1994). "Double-pulse electronic interferometry for vibration analysis." Optical Society of America.

Perez-Gracia, V. (2008). "Horizontal resolution in a non-destructive shallow GPR survey: an experimental evaluation." NDT & E International 41: 611-620.

Pieraccini, M., M. Fratini, F. Parrini, G. Macaluso, C. Atze ni.(2004). "High-speed CW step-frequency coherent radar for dynamic monitoring of civil engineering structures." Electronics Letters 40(14): 907-908.

Pieraccini, M., G. Luzi, D. Mecatti, M. Fratini, L. Noferini, L. Carissimi, G. Franchioni, C. Atzeni, (2004). "Remote sensing of building structural displacements using a microwave interferometer with imaging capability." NDT & E International 37(7): 545-550.

Prado, P. J., B. J. Balcom, S. D. Beyea, R. L. Armstrong, T. W. Bremner. (1997). "Concrete thawing studied by single-point ramped imaging." Solid State Nuclear Magnetic Resonance 10(1-2): 1-8.

Rao, M. R. P. D. (2007). Review of nondestructive evaluation techniques for FRP composite structural components. Department of Civil and Environmental Engineering. Morgantown, WV, West Virginia University. Master of Science in Civil Engineering: 225.

Rice, C., S.-E. Chen, K. Dai, W. Liu, R. Eguchi, E. Hauser, C. Boyle, B. Phibrick. (2010). Remote sensing techniques for bridge inspections. Transportation Research Board 89th Annual Meeting. Washington, D.C., Transportation Research Board of IHF National Academies.

Roth, D. J., L. M. Cosgriff, R. E. Martin, M. J. Verrilli, R. T. Bhatt.(2003). Microstructural and defect characterization in ceramic composites using an ultrasonic guided wave scan system. 30th Annual Review of Quantitative Nondestructive Evaluation (QNDE). Green Bay, WI, U.S.A.

Ryan, T. W., R. A. Hartle, J. E. Mann, L. J. Danovich. (2006). "Bridge Inspector's Reference Manual." (FHWA NHI 03-001).

Santulli, C. (2000). Impact damage evaluation in woven composites using acoustic and thermoelastic techniques. Department of Engineering. Liverpool, U.K., University of Liverpool. Doctor of Philosophy: 253.

Schueler, R., S. P. Joshi, K. Schulte. (2001). "Damage detection in CFRP by electrical conductivity mapping." Composites Science and Technology 61(6): 921-930.Singh, V., G. M. Lloyd, M. L. Wang.(2004). "Effects of temperature and corrosion thickness and composition on magnetic measurements of structural steel wires." NDT & E International 37(7): 525-538.

Song, G., Y. L. Mo, K. Otero, H. Gu.(2006). "Health monitoring and rehabilitation of a concrete structure using intelligent materials." Smart Materials and Structures 15(2): 309.

Steckenrider, J. S. and J. W. Wagner (1995). "Computed speckle decorrelation (CSD) for the study of fatigue damage." Optics and Lasers in Engineering 22(1): 3-15.

Stepanova, L. N., E. Y. Lebedev, A. E. Kareev, V. N. Chaplygin, S. A. Katarushkin.(2004). "Use of the acoustic emission method in detecting the fracture process in specimens made of composite materials." Russian Journal of Nondestructive Testing 40(7): 455-461.

Stephen, V., S. Kharkovsky, J. Nadakuduti, R. Zoughi.(2004). "Microwave field measurement of delaminations in CFRP concrete members in a bridge." Journal of Materials in Civil Engineering.

Sumitro, S., A. Jarosevic, M. L. Wang.(2002). "Elasto-magnetic sensor utilization on steel cable stress measurement."

Tanner, N. A., J. R. Wait, C. R. Farrar, H. Sohn.(2003). "Structural health monitoring using modular wireless sensors." Journal of Intelligent Material Systems and Structures 14.

USDOT (2001). Highway Bridge Inspection: State-of-the-Practice Survey. T.-F. H. R. Center. Mclean, VA, U.S.A., U.S. Department of Transportation, Federal Highway Administration.

Van der Kruk, J. (2003). "Three-dimensional GPR imaging in the horizontal wavenumber domain for different heights of source and receiver antennae."

Wen, S. and D. D. L. Chung (2000). "Damage monitoring of cement paste by electrical resistance measurement." Cement and Concrete Research 30(12): 1979-1982.

Whelan, M. J., M. V. Gangone, K. D. Janoyan, K. Cross, R. Jha.(2007). "Reliable high-rate bridge monitoring using dense wireless sensor arrays." 8.

Winfree, W. P. (1998). "Enhanced thermographic detection of delaminations with computational pulse shaping." Review of Progresss in Quantitative Nondestructive Evaluation 17A: 441-447.

Yu, X. and X. Yu (2009). "Time domain reflectometry automatic bridge scour measurement system: principles and potentials." Structural Health Monitoring 8(6): 463-476 10.1177/1475921709340965: 10.1177/1475921709340965.

Zhang, G., R. S. Harichandran, P. Ramuhalli.(2010). NDE of concrete bridge deck delamination using enhanced acoustic method. Transportation Research Board 89th Annual Meeting. Washington, D.C., Transportation Research Board of IHF National Academies.

Zhang, Z. Y. and M. O. W. Richardson (2005). "Visualisation of barely visible impact damage in polymer matrix composites using an optical deformation and strain measurement system (ODSMS)." Composites Part A: Applied Science and Manufacturing 36(8): 1073-1078.

Zilberstein, V., K. Walrath, D. Grundy, D. Schlicker, N. Goldfine, E. Abramovici, T. Yentzer.(2003). "MWM eddy-current arrays for crack initiation and growth monitoring." International Journal of Fatigue 25(9-11): 1147-1155.